Section 2 Plasma Physics

Chapter 1 Plasma Dynamics

Chapter 1. Plasma Dynamics

Academic and Research Staff

Professor George Bekefi, Professor Abraham Bers, Professor Bruno Coppi, Professor Miklos Porkolab, Professor Jonathan S. Wurtele, Dr. Kuo-in Chen, Dr. Shien-Chi Chen, Dr. Thomas Dupree, Dr. Ronald C. Englade, Dr. Stanley C. Luckhardt, Dr. Stefano Migliuolo, Dr. Abhay K. Ram, Dr. Linda E. Sugiyama, Edward W. Fitzgerald, Ivan Mastovsky

Visiting Scientists and Research Affiliates

Jean-Loup Delcroix,[1] Paolo Detragiache,[2] Lazar Friedland,[3] Vladimir Fuchs,[4] Dr. Eli Jerby,[5] Dr. Chaim Leibovitch,[7] Dr. Marco Nassi[6] Dr. Kongyi Xu[8]

Graduate Students

Riccardo Betti, Carson Chow, Stefano Coda, Jeffrey A. Colborn, Manoel E. Conde, Christian E. de Graff, Anthony C. DiRienzo, Darin Ehrnst, Mark Jablonski, Robert J. Kirkwood, Kenneth C. Kupfer, Alberto Leon, Jared P. Squire, Richard E. Stoner, Jesus N.S. Villasenor

Undergraduate Students

Daniel P. Aalberts, George Chen, Salvatore DiCecca, Weng-Yew Ko, John A. Marroquin, Kurt A. Schroder, Peter Woo

Technical and Support Staff

Ann Dix, Laura B. Doughty, Toni Fischer, Catherine Lorusso

1.1 Relativistic Electron Beams

Sponsors

Lawrence Livermore National Laboratory
Subcontract 6264005
National Science Foundation
Grants ECS 84-13173 and ECS 85-14517
U.S. Air Force - Office of Scientific Research
Contract AFOSR 84-0026
U.S. Army - Harry Diamond Laboratories
Contract DAAL02-86-C-0050
U.S. Navy - Office of Naval Research
Contract N00014-87-K-2001

Project Staff

Professor George Bekefi, Professor Jonathan S. Wurtele, Manoel E. Conde, Christian E. de Graff, Richard E. Stoner, Anthony C. DiRienzo, Daniel P. Aalberts, Salvatore DiCecca, Dr. Kongyi Xu, Dr. Chaim Leibovitch, Dr. Eli Jerby, Ivan Mastovsky, Dr. Shien-Chi Chen

---

[1] University of Paris, Orsay, and Ecole Superieure d'Electricite, France.

[2] University of Turin, Torino, Italy.

[3] Hebrew University of Jerusalem, Israel.

[4] IREQ, Quebec, Canada.

[5] Tel Aviv University, Tel Aviv, Israel.

[6] Politecnico di Milano, Milan, Italy.

[7] Rafael Laboratory, Haifa, Israel.

[8] China University of Electronic Science and Technology, Chengdu, People's Republic of China.

1.1.1 Coherent Free-Electron Radiation Sources

The possibility of developing lasers and masers in which the active medium is a stream of free electrons has evoked much interest in recent years. The potential advantages are numerous, including continuous frequency tuning through variation of the electron energy and very high-power operation. In comparison with solid, liquid and gas lasers, little damage can occur to this lasing medium.

Interestingly, these novel sources and the underlying physical mechanisms have much more in common with the earliest sources of coherent electromagnetic radiation (namely the various microwave devices) than they have with the more recent atomic and molecular lasers. Indeed, the klystron, the magnetron, and the traveling wave tube conceived and developed in the 1940s and 50s are examples of free-electron sources capable of generating coherent microwave radiation. In the decameter and centimeter wavelength ranges, these devices can emit at power levels as high as tens of megawatts with good efficiencies exceeding 60 percent. Today, these systems and their variations have become indispensable instruments of modern science, technology and communication.

With the new generation of free-electron sources, we and others aim to extend the electromagnetic spectrum from the microwave to the millimeter, infrared, visible, and ultraviolet regimes with previously unattainable intensities and efficiencies. Potential applications include spectroscopy in condensed matter physics and in atoms and molecules, isotope separation, development of novel accelerators, millimeter and submillimeter wavelength radar and communication, heating of thermonuclear fusion plasma, biomedicine, and lithography.

Free electron lasers are large and expensive because their size and cost increase as the radiation wavelength decreases. Therefore, facilities are now limited to a few large laboratories. However, a number of novel concepts to reduce their size and cost are being explored at various institutions. One is the design and construction of novel, compact accelerators such as the high-gradient rf linacs powered by intense millimeter wavelength rf drivers. Acceleration gradients in excess of several hundred MeV per meter length may be possible. At present we are studying the performance of such structures operating at a frequency of 35 GHz (see figure 1).

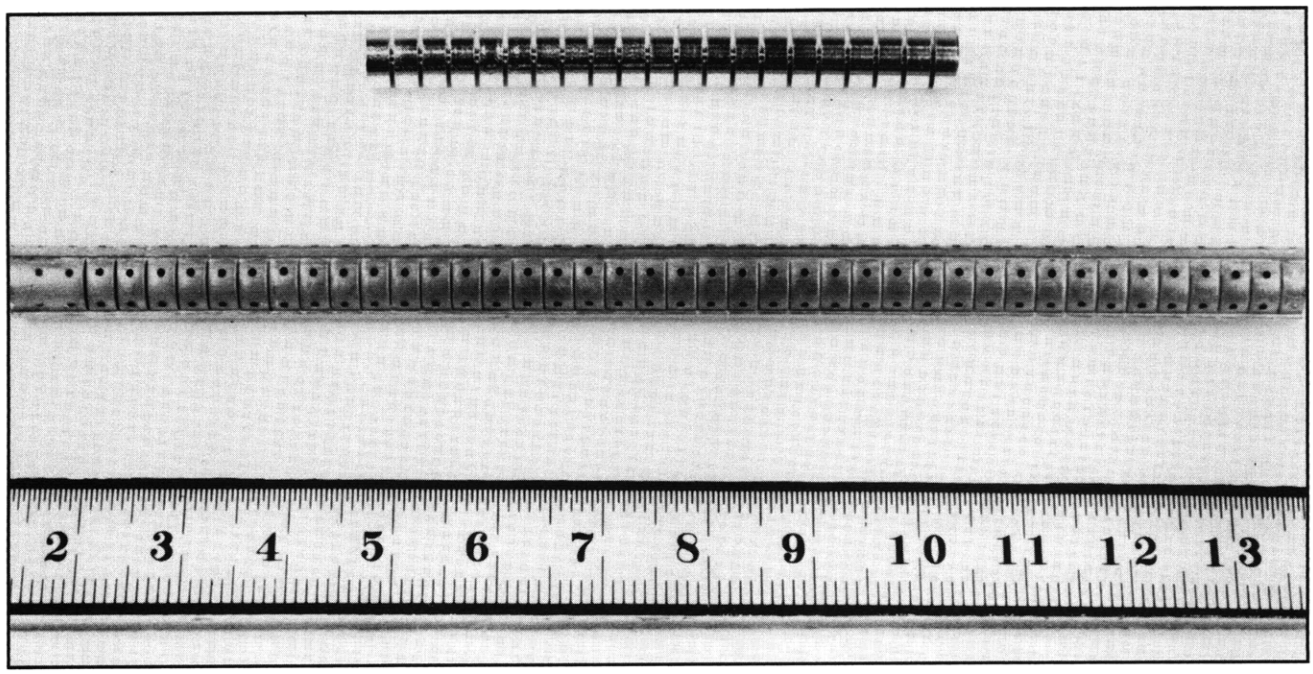

Figure 1.

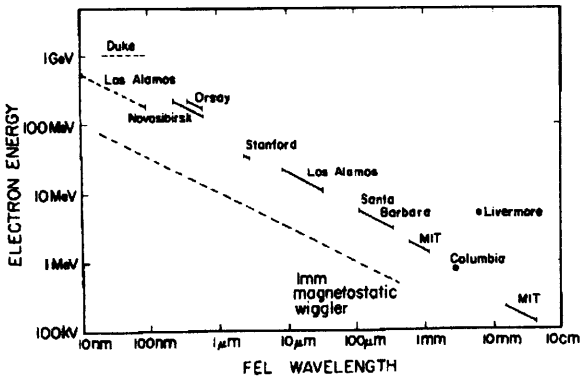

Figure 2.

The design and construction of novel, short-period wigglers is being examined at a number of research centers. Figure 2 illustrates which facilities are presently using conventional wigglers. The fact that all the existing FELs lie, for the most part, on a single straight line of the voltage versus wavelength graph implies that they all use wigglers with roughly the same periodicity, l_w. This is indeed the case with l_w ranging between ~3 and ~5 cm. A reduction of l_w by a factor of ten, for instance, leads to a reduction in wiggler length by 10 and a reduction in accelerator voltage by $\sqrt{10}$. The overall effect is a smaller accelerator, a shorter wiggler, and less stringent requirements on radiation shielding.

Many different designs are under scrutiny at present, as indicated in figure 3. Plotted along the vertical axis of figure 3 is the wiggler strength expressed in terms of the normalized vector potential defined as

$$a_w = \frac{eB_w}{m_0 k_w c} \simeq 0.1 B_w(\text{kG}) l_w(\text{cm}).$$

Since the FEL gain increases with increasing a_w, large a_w (≥ 1) is desirable, but difficult to achieve. Figure 3 shows that if the wiggler periodicity, l_w, is shorter, a_w tends to be smaller.

At MIT, we have tested prototype microwigglers with a period of 2.4 mm and 10 mm. A 70-period version is now under construction. When completed, it will be used in a collaborative effort on the 50-MeV rf linac at Brookhaven National Laboratory to produce coherent light at 0.47 μm wavelength.

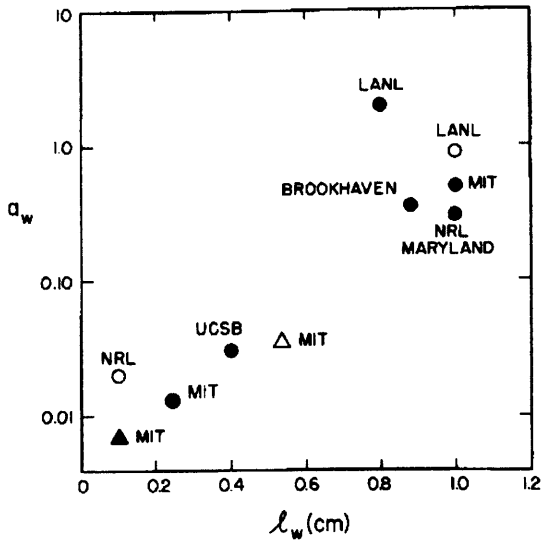

Figure 3.

1.2 Plasma Wave Interactions — RF Heating and Current Generation

Sponsors

National Science Foundation
Grants ECS 85-15032 and ECS 88-22475
U.S. Department of Energy
Contract DE-AC02-ET-51013

Project Staff

Professor Abraham Bers, Dr. Abhay K. Ram, Carson Chow, Mark Jablonski, Kenneth C. Kupfer, Jean-Loup Delcroix, Vladimir Fuchs, Lazar Friedland

1.2.1 Introduction

The research work of this group is concerned with studies on the electrodynamics of plasmas. Particular attention is directed toward understanding wave propagation and the nonlinear dynamics of plasmas driven by high frequency electromagnetic fields for plasma heating and/or current generation within the plasma.

In the following sections, we report on our progress on the following topics:

1. Particle and energy diffusion induced by intense RF fields. This entails a new description of such transport using nonlinear dynamics techniques of induced stochasticity and chaos, and is reported in Section 1.2.2, "Transport in Intense RF Fields."

2. Wave propagation and mode conversion in ion-cyclotron heating for high-temperature, magnetically confined plasmas. We report on an analytic description of the reflection coefficient in mode conversion (Section 1.2.3, "The Reflection Coefficient in Ion-Cyclotron Heating" on page 171), on optimizing the energy deposition on ions in the mode conversion region (Section 1.2.4, "Optimizing the Absorption in Ion-Cyclotron Heating" on page 173), and on kinetic ray tracing of the mode converted waves (IBW) and their energy deposition on electrons (Section 1.2.5, "Propagation of Mode Converted Ion-Bernstein Waves in Toroidal Plasmas" on page 174).

3. Frequency locking and chaos in self-oscillating (linearly unstable) dynamics — a generic study of the combined van der Pol and Duffing oscillator nonlinearities (Section 1.2.6, "Dynamics of a Forced van der Pol-Duffing Oscillator" on page 176).

1.2.2 Transport in Intense RF Fields

We are studying the guiding center motion of charged particles interacting with electrostatic waves in a tokamak. This motion is described by a time dependent Hamiltonian in a four-dimensional phase space composed of the guiding center's three position coordinates and its parallel velocity (along the magnetic field). This is a generalization of previous studies in which either the drift motion[9] or the parallel wave fields have been ignored.[10] In our approach, we obtain diffusion of the guiding center parallel velocity and its radial position when the wave amplitudes exceed a threshold value for the onset of stochastic motion.[11]

Using the guiding center Lagrangian[12] to describe the motion in an axisymmetric, time-independent equilibrium, the Hamiltonian describing the motion is given by:

$$H = \frac{m}{2} u^2 + MB(\psi, \theta) + e\Phi(\psi, \theta, \phi, t), \quad (1)$$

where M is the magnetic moment of a particle of mass m and charge e, Φ is the scalar potential of the imposed wave field, u is the parallel velocity of the guiding center and $B = |\mathbf{B}|$ is the magnetic field. The tokamak geometry is described by (ψ, θ, ϕ), where ψ is the usual poloidal flux function and ϕ is the toroidal angle. The coordinate θ is chosen so that $\nabla\theta$ is perpendicular to both $\nabla\psi$ and $\nabla\phi$. In order to analyze the dynamics of the charged particles, it is convenient to transform the above coordinates to action-angle coordinates of the unperturbed Hamiltonian. Then the Hamiltonian can be written as:

$$H = H_o(I_\phi, I_\theta) + \Phi(I_\phi, I_\theta, \zeta_\phi, \zeta_\theta, t) \quad (2)$$

---

[9] V. Fuchs, V. Krapchev, A.K. Ram, and A. Bers, "Diffusion of Electrons by Coherent Wavepackets," *Physica* 14D: 141-160 (1985); A.K. Ram, K. Hizanidis, and A. Bers, "Trapped-Electron Stochasticity Induced by Frequency-Modulated Waves," *Phys. Rev. Lett.* 56 (2):147-150 (1986).

[10] R.G. Kleva and J.F. Drake, "Stochastic E x B Particle Transport," *Phys. Fluids* 27 (7): 1686-1698 (1984); W. Horton and D.I. Choi, "Electron Diffusion in Tokamaks Due to Electromagnetic Fluctuations," *Plasma Phys. Contr. Fusion* 29 (7): 901-918 (1987).

[11] K. Kupfer, A. Bers, and A.K. Ram, "Guiding Center Stochasticity by Electrostatic Waves in Toroidal Geometry," (abstract) *Bull. Am. Phys. Soc.* 34: 1927 (1989).

[12] R.G. Littlejohn, "Variational Principles of Guiding Centre Motion," *J. Plasma Phys.* 29: 111-125 (1983).

where I_ϕ is the toroidal action, I_θ is the poloidal action and ζ_ϕ and ζ_θ are the canonical angles, respectively. We have used this approach to study the stochasticity, including radial diffusion, of super-thermal electrons during lower-hybrid current drive (LHCD). A majority of the electrons interacting with the waves are not trapped by the toroidal magnetic field so we have explicitly evaluated the action-angle transformation for circulating electrons in a low β, circular equilibrium. The transformed potential is a periodic function of the angles ζ_ϕ and ζ_θ, so we write it as a Fourier series with respect to these coordinates:

$$\Phi = \mathrm{Re}\{\Sigma C_{n,\ell}(\mathbf{I})\, e^{i(n\zeta\phi + \ell\zeta\theta - \omega t)}\} \qquad (3)$$

where the sum is over all n and ℓ, ω is the frequency of the source, and $\mathbf{I} = (I_\phi, I_\theta)$. We consider an ensemble of randomly phased waves in the plasma. The spectrum is assumed to be finite for $n_1 \leq n \leq n_2$. Typically LHCD experiments have broad spectra where n_2 is approximately twice n_1, and n_1 is about 10^2. The amplitude of the RF field is large enough that the trapping widths of the resonances in action space satisfy the overlap criterion, creating a broad region of connected stochasticity. The quasi-linear diffusion tensor in action space is[13]

$$D_{i,j}(\mathbf{I}) = \Sigma \frac{\pi}{2} |C_{n,\ell}(\mathbf{I})|^2 \delta(R_{n,\ell}(\mathbf{I})) \Pi_{i,j}(n,\ell) \quad (4)$$

where $R_{n,\ell}(\mathbf{I}) = n\Omega_\phi + \ell\Omega_\theta - \omega = 0$ is the resonance curve in action space and Ω_ϕ and Ω_θ are the linear frequencies determined by differentiating $H_o(\mathbf{I})$ with respect to each component of the action, I_ϕ and I_θ. The components of the $\Pi_{i,j}$ tensor are: $\Pi_{\phi,\phi} = n^2$, $\Pi_{\phi,\theta} = \Pi_{\theta,\phi} = \ell n$, and $\Pi_{\theta,\theta} = \ell^2$. Although $D_{i,j}(\mathbf{I})$ is a singular tensor field it should be smoothed out by coarse graining action space because the resonances are broadened by small nonlinearities (i.e., they have finite trapping widths). We have computed the coarse-grained $D_{i,j}(\mathbf{I})$ numerically, with the spectrum, $C_{n,\ell}$, obtained by transforming the assumed RF field into action-angle coordinates. The results of this calculation have been compared to numerical computations of the non-linear equations of motion obtained directly from the Hamiltonian in (1). Agreement is achieved when the amplitude of the RF field is small enough so that the trapping width of each resonance in action space is small compared to the width of the stochastic region. In this case, the basic scaling for the radial diffusion is D_{RF}/ω_{ce}^2, where D_{RF} is the average RF quasi-linear diffusion coefficient in parallel velocity and ω_{ce} is the electron cyclotron frequency. In typical LHCD experiments, D_{RF} is large enough so that the associated RF radial diffusion dominates classical collisional diffusion for the super-thermal electrons. The quasi-linear approximation overestimates the diffusion at larger amplitudes.

1.2.3 The Reflection Coefficient in Ion-Cyclotron Heating

The ICRH problem in a tokamak plasma, which can be formulated in general as an integro-differential equation, has usually been approximated by a fourth- or sixth-order differential equation and solved numerically. However, in order to make predictions and to better understand the scaling laws (see Section 1.2.4, following), it is important to have closed form solutions of the scattering coefficients for the mode-conversion region. Over the past two to three years, we have worked toward an approximate analytic description of the RF power transmission (T), reflection (R), mode-conversion (C), and kinetic dissipation (D) coefficients for ICRH. To achieve our goal, we have used the technique of "order reduction" whereby the fourth or higher order differential equations are reduced to combinations of lower order equations that retain the essential physics of the complete problem. So far, we have obtained a first-order differential equation for

[13] A.N. Kaufman, "Quasilinear Diffusion of an Axisymmetric Toroidal Plasma," *Phys. Fluids* 15 (6): 1063-1069 (1972).

T,[14] and a set of coupled equations, which include the effects of kinetic dissipation, for C and T.[15] These equations can be solved analytically to obtain C and T. A second order equation has also been found for R and T.[16] Until recently, this equation, known as the "fast wave approximation," was solved numerically to find R. We have now found a closed form solution for R. Thus, for all heating scenarios of current interest,[17] [D – (H), D – (^{3}He)], we have closed form solutions for all of the scattering coefficients using this order reduction technique.

The following is a summary of our new result for R. The approximate fast wave equation[18] is a second-order, ordinary differential equation with a complex potential and, in general, has no closed-form, analytic solution. However, we noted that the real part of the potential looks like a resonance broadened "Budden" potential. The imaginary part has two peaks: one peak corresponds to the "Budden" like potential, the other to the ion-cyclotron resonance. The "Budden" part includes the effects of mode conversion to the ion-Bernstein wave and any dissipation that may be present in that particular process. To solve for R and T, we approximate the complex potential by the Budden potential, for which analytic solutions exist.[19] The ion cyclotron part is then treated as a perturbation which affects a slowly varying amplitude on the asymptotic Budden solutions. We obtain

$$T = e^{-\pi s_0} e^{-2\mu},$$

$$R = e^{-4\mu} e^{-4\nu} (1 - T^2)^2,$$

$$\mu = \left| \int_0^\infty \frac{g(s)}{2} \, ds \right| \qquad (1)$$

where $\nu = \sqrt{\pi}\, N_c \gamma \varepsilon_r / \tau^2$, g(s) is the imaginary part of the complex potential, $s_0 = N_c^3 \gamma/(2\tau + \lambda_N)^2$, and all the other quantities are given in Chow et al.[20] T in (1) checks with our previous, independent derivations for T. R in (1) has been compared with the numerical results generated by the codes of D. Smithe (PPPL) and E.F. Jaeger (ORNL). The results agree very well over a wide range of parallel wavenumbers for heating scenarios of current interest for Alcator C-mod and CIT. A detailed derivation and comparison of the results has been recently submitted to *Phys. Fluids B*.[21]

---

[14] G. Francis, *Coupled-Mode Propagation and Instability in Inhomogeneous Plasmas,* Ph.D. diss., Dept. of Physics, MIT, 1987; G. Francis, A. Bers, and A.K. Ram, "Non-Resonant Mode-Coupling Model of ICRF Heating," in *Proceedings of the 7th Topical Conference on Applications of RF Power to Plasmas,* A.I.P. Conf. Proc. 159, eds. S. Bernabei and R.W. Motley, 370-373, (New York: 1987).

[15] V. Fuchs and A. Bers, "Dissipative Mode Coupling in Ion-Cyclotron Resonance Minority Heating," *Phys. Fluids* 31 (12): 3702-3708 (1988). Note the following misprints: On line before (17a), $K_1 \sim \varepsilon$ should read $K'_1 \sim \varepsilon$; in second expression of (20) replace K_0 with $-K_0$; r.h.s. of (25) should have be multiplied by a factor of 2.

[16] C. Lashmore-Davies, V. Fuchs, G. Francis, A.K. Ram, A. Bers, and L. Gauthier, "A Theory of Fast-Wave Absorption, Transmission, and Reflection in the Ion-Cyclotron Range of Frequencies," *Phys. Fluids* 31 (6): 1641-1622 (1988).

[17] C. Chow, A. Bers, and V. Fuchs, "Analytic Studies of ICRF Heating," in *Radio Frequency Power in Plasmas,* A.I.P. Conf. Proc. 190, ed. R. McWilliams, 234-237, (New York: American Institute of Physics, 1989). Note the following misprints: In Section III, the expression for K_0 is missing a term $-N_\parallel^2$; in Section IV, in the expression for ν replace $-N_\parallel^2$ by $+N_\parallel^2$].

[18] C. Lashmore-Davies et al., *Phys. Fluids* 31 (6): 1641-1622 (1988).

[19] R.B. White and F.F.Chen, "Amplification and Absorption of Electromagnetic Waves in Overdense Plasmas," *Plasma Phys.* 16: 565-587 (1974).

[20] C. Chow et al. A.I.P. Conf. Proc. 190: 234-237 (1989).

[21] C. Chow, V. Fuchs, and A. Bers, *Reflection at the Resonance Layer of the Fast Alfvén Wave in Ion Cyclotron Heating,* Plasma Fusion Center Report PFC/JA-90-2 (Cambridge: MIT, 1989).

1.2.4 Optimizing the Absorption in Ion-Cyclotron Heating

In view of the results described in Section 1.2.3, we can now use a global power conservation (i.e., integrating over a volume of the plasma extending into the asymptotic regions away from the mode-conversion region) to determine the power dissipated (D):

- For a fast Alfvén wave (FAW) incident from the low-B_0 side,

$$T + R + C_L + D_L = 1 \qquad (1)$$

- For a FAW incident from the high-B_0 side,

$$T + C_H + D_H = 1 \qquad (2)$$

where the subscripts L and H stand for, respectively, low- and high-B_0 incidence. (Note that T is the same, and $R_L = R$, while $R_H = 0$). With these results, we can then find the plasma and RF heating parameter space for optimizing ion-cyclotron heating in tokamak plasmas. We summarize this in the following, with notation that we have used before.[22]

Consider incidence of a FAW from the low-B_0 side of the tokamak. Note that the conversion coefficient[23] can be written as

$$C_L = \frac{1}{2\pi} f(\Lambda) T^{1/2} R\, e^{-2D_c} \qquad (3)$$

where $f(\Lambda) \equiv |\Lambda|\,|\Gamma(-i\Lambda)|^2$. Now consider small $N_\parallel$ (Alfvén parallel index, $c_A k_\parallel/\omega$) so that the Z-functions that enter into (3) can be taken in their asymptotic limits. Then Λ is approximately real and (3) becomes

$$C_L \approx \frac{e^{-\pi\Lambda}}{2\sinh\pi\Lambda} R\, e^{-2D_c} \qquad (4)$$

We now choose $\Lambda > 1$ so that both $T \approx 0$ and $C_L \approx 0$ in the range of small $N_\parallel$ of interest. This

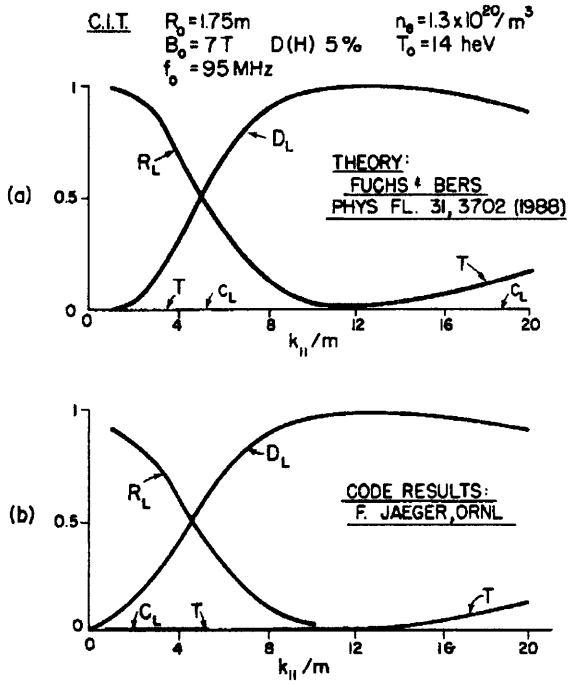

Figure 4. Power scattering coefficients for low-B_0 incidence of a FAW for CIT-type plasma. (a) Theory. (b) Numerical code results.

choice gives us a relation between η (the minority species concentration), R_A (the plasma major radius in units of Alfvén wavelengths), and β_i (the plasma ion beta). Then from (1) we have

$$R + D_L \approx 1 \qquad (5)$$

It can readily be shown (see Section 1.2.3, preceding) that R decreases exponentially with $R_A N_\parallel^2$ so that, according to (5), as $N_\parallel$ increases, the dissipation coefficient D_L increases to unity. We can thus establish a relationship between $N_\parallel^2$, R_A and β_i so that $D_L \approx 1$ and $R \approx 0$. This achieves the goal of single-pass absorption. Note that by these means one can approximately determine the optimum η and $N_\parallel$ for a given set of β_i and R_A.

[22] C. Chow et al. A.I.P. Conf. Proc. 190: 234-237 (1989).

[23] V. Fuchs and A. Bers, *Phys. Fluids* 31(12): 3702-3708 (1988).

Figure 4 shows a computation (for CIT-type parameters) based upon the approximate analytic formulas obtained for T, R, and C_L. The results are in excellent agreement with the T, R, and C_L obtained from a numerical solution of the fourth-order differential equation (numerical results: courtesy of F. Jaeger, ORNL). Note that in this case, for low-B_0 incidence of a FAW, we have indeed a situation in which at low $N_\parallel$'s $T \approx 0$, $C_L \approx 0$, and the interplay between reflection and dissipation is as given by (5).

Finally, note that for high-B_0 incidence of a FAW, there is a similar interplay between C_H and D_H, but at higher $N_\parallel$'s. This can be understood from the fact that, approximately[24]

$$C_H \approx 2 \sinh \pi\Lambda \, e^{-\pi\Lambda} e^{-2D_c} \qquad (6)$$

so that for $\Lambda > 1$ we have again $T \approx 0$, and from (6), $C_H \approx \exp(-2D_c)$. Thus, equation (2) becomes

$$C_H + D_H \approx 1 \qquad (7)$$

The kinetic dissipation in mode conversion D_c, increases with $N_\parallel$, and hence $C_H \to 0$ and, by (7), $D_H \to 1$. Thus, we have complete dissipation, although at a higher $N_\parallel$ than before, also for high-B_0 incidence. Figure 5 shows a computation (also for CIT-type parameters), based upon the approximate analytic formulas obtained for T and C_H, and compares them with the numerical results obtained from the fourth-order o.d.e. code mentioned above. Again the results are in excellent agreement, exhibiting the interplay between C_H and D_H as described in (7).

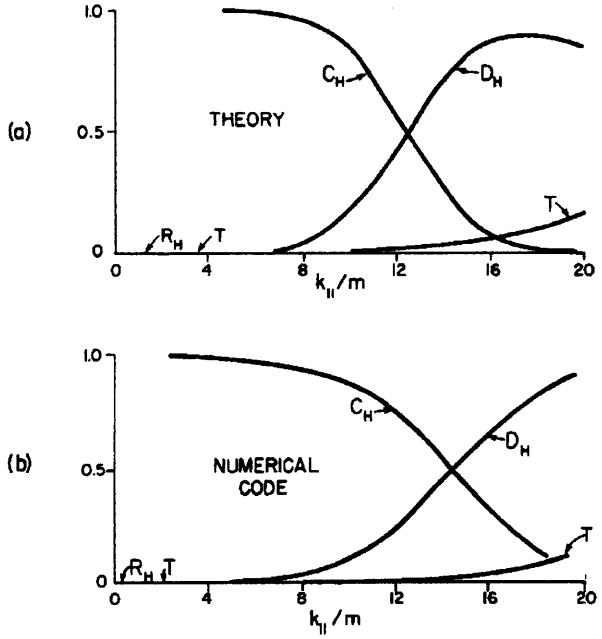

Figure 5. Power scattering coefficients for high-B_0 incidence of a FAW. Plasma parameters are the same as in figure 4. (a) Theory. (b) Numerical code results.

1.2.5 Propagation of Mode Converted Ion-Bernstein Waves in Toroidal Plasmas

For small values of $k_\parallel$ (the component of the wave number parallel to the magnetic field in a tokamak), the fast Alfvén wave can effectively excite the ion-Bernstein wave (IBW) during ICRF heating of tokamak plasmas. This occurs near the ion-ion hybrid resonance layer in a plasma consisting of two ion species. The amount of power coupled to low values of $k_\parallel$ is significant for single antennas at the edge of the plasma which excite fast Alfvén waves that propagate into the plasmas. We have been studying the propagation characteristics of this IBW in a toroidal plasma. Toward this end, we have developed a numerical code which solves for the propagation characteristics of rays in

[24] Ibid.

three-dimensional toroidal equilibria.[25] The local dispersion function, $D(\vec{k}, \omega, \vec{r})$, used for following the rays is obtained from the fully electromagnetic *hermitian* dielectric tensor[26] describing a kinetic, hot Maxwellian plasma. Here $\vec{r} = (r, \theta, \phi)$ is the position vector where r is the radius measured from the magnetic axis of the torus, θ is the poloidal angle, and ϕ is the toroidal angle; $\vec{k} = (k_r, m, n)$ is the wave vector with components k_r, m and n in the radial, poloidal and toroidal directions, respectively; and ω is the frequency. The spatial profiles of the density, temperature, and the magnetic field components are included, in a WKB sense, explicitly in D. Besides the usual ray trajectory equations:

$$\frac{d\vec{k}}{dt} = \frac{(\partial D/\partial \vec{r})}{(\partial D/\partial \omega)}, \quad \frac{d\vec{r}}{dt} = -\frac{(\partial D/\partial \vec{k})}{(\partial D/\partial \omega)} \qquad (1)$$

the numerical code also solves for the variation of the wave energy density, U, along the rays:[27]

$$\frac{\partial U}{\partial t} + \nabla \cdot \left(\frac{\partial \omega}{\partial \vec{k}} U \right) + \frac{1}{2} \bar{\bar{\sigma}}^H : \vec{a}\vec{a}^* = 0 \qquad (2)$$

where $\bar{\bar{\sigma}}^H$ is the hermitian part of the conductivity tensor and $\vec{a}$ is the slowly varying (complex) part of the electric field of the wave. The relation between U and $\vec{a}$ is given by:

$$U = \frac{1}{16\pi} \frac{\partial(\omega \bar{\bar{D}})}{\partial \omega} : \vec{a}\vec{a}^* ; \qquad (3)$$

$$\bar{\bar{D}} = (1 - \frac{c^2 k^2}{\omega^2})\bar{\bar{I}} + \frac{c^2 \vec{k}\vec{k}}{\omega^2} + \frac{4\pi i \bar{\bar{\sigma}}^A}{\omega}$$

where $\bar{\bar{\sigma}}^A$ is the anti-hermitian part of the conductivity tensor, $k^2 = \vec{k} \cdot \vec{k}$, c is the speed of light, $\bar{\bar{I}}$ is the unit tensor, and $\det(\bar{\bar{D}}) = D(\vec{k}, \omega, \vec{r})$. The second term in equation (2) describes changes associated with the convergence and divergence of a bundle of rays, and the third term describes changes in U due to damping of the wave energy on the particles.

A numerical analysis of the propagation of ion-Bernstein waves shows that they can effectively damp onto the electrons. The rate of damping, and the spatial location where the damping takes place, is determined primarily by, $\tilde{B}$, the ratio of the poloidal magnetic field to the total magnetic field. For large values of $\tilde{B}$ the IBW damp onto the electrons close to the ion-ion hybrid resonance layer. As $\tilde{B}$ is decreased, the IBW damp out closer to the edge of the tokamak in the high toroidal magnetic field and low density and temperature regimes. The damping is a consequence of an upshift in |m| leading to a subsequent enhancement in $|k_\parallel|$. The change in m over a radial distance of propagation Δr in a hydrogen-deuterium plasma (with hydrogen as a minority species) is approximately given by[28]

$$\Delta m \approx \frac{2}{3} \frac{\omega_{cd}^2}{k_r v_{td}^2} \left(2 + 11 \frac{v_{td}^2}{c^2} \frac{\omega_{pd}^2}{\omega_{cd}^2} \right) \frac{r \sin\theta}{(R + r\cos\theta)} \Delta r \qquad (4)$$

where $\omega_{cd}(\omega_{pd})$ is the local deuterium cyclotron (plasma) frequency, and v_{td} is the deuterium thermal velocity. This formula shows that the enhancement in m is not unidirectional. The direction of the upshift is determined by the horizontal axis of symmetry of the plasma. Above this axis the

---

[25] A.K. Ram and A. Bers, "Kinetic Ray Tracing in Toroidal Geometry with Applications to Mode-Converted Ion-Bernstein Waves," in *Proceedings of the 1989 Conference on Plasma Physics,* New Delhi, India, 57-60, eds. A. Sen and P.K. Kaw (1989).

[26] A. Bers, "Linear Waves and Instabilities," in *Plasma Physics — Les Houches 1972,* eds. C. DeWitt and J. Peyraud (New York: Gordon and Breach, 1972); I.B. Bernstein and L. Friedland, "Geometric Optics in Space and Time Varying Plasmas," in *Handbook of Plasma Physics,* Vol. 1, eds. M.N. Rosenbluth and R.Z. Sagdeev (New York: North Holland Pub. Co., 1983).

[27] Ibid.

[28] A.K. Ram and A. Bers, *Proceedings of the 1989 Conference on Plasma Physics,* New Delhi, India (1989).

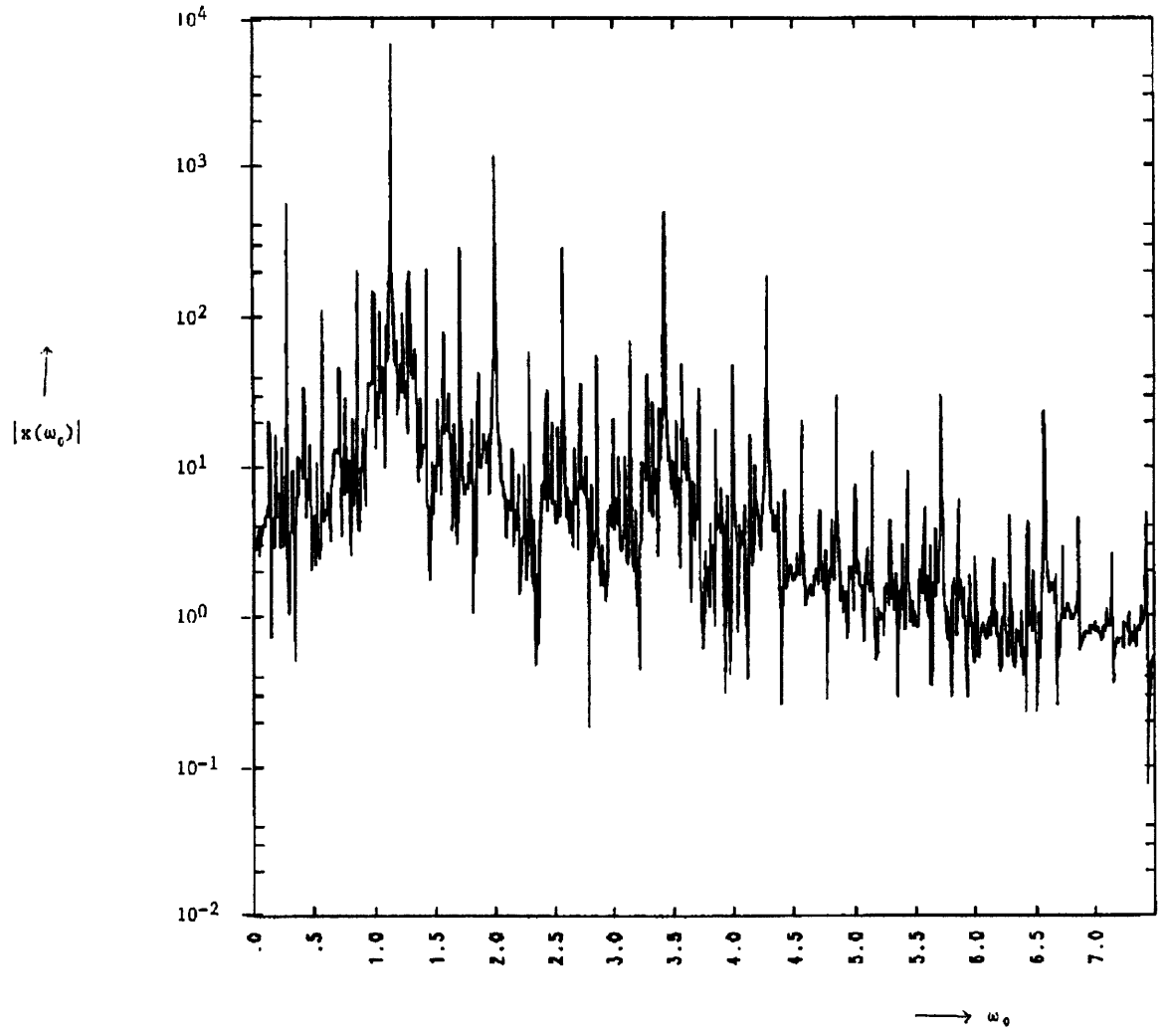

Figure 6. The frequency spectrum of x for the quasi-periodic case ($\varepsilon = 0.51$).

upshift is towards larger negative values and below the axis the upshift is towards larger positive values. Consequently, ion-Bernstein waves are not good candidates for driving plasma currents.

1.2.6 Dynamics of a Forced van der Pol-Duffing Oscillator

The phenomena of frequency locking and quasi-periodic behavior in physical systems, which are described by nonlinear ordinary differential equations in time and exhibit nonlinear oscillations, is well-known.[29] Study of the occurrence of chaos in physical systems, on the other hand, is more recent. Frequency locking occurs in self-oscillatory systems (i.e., systems that oscillate in the

[29] See for example: C. Hayashi, *Nonlinear Oscillations in Physical Systems* (New York: McGraw Hill Book Co., 1964).

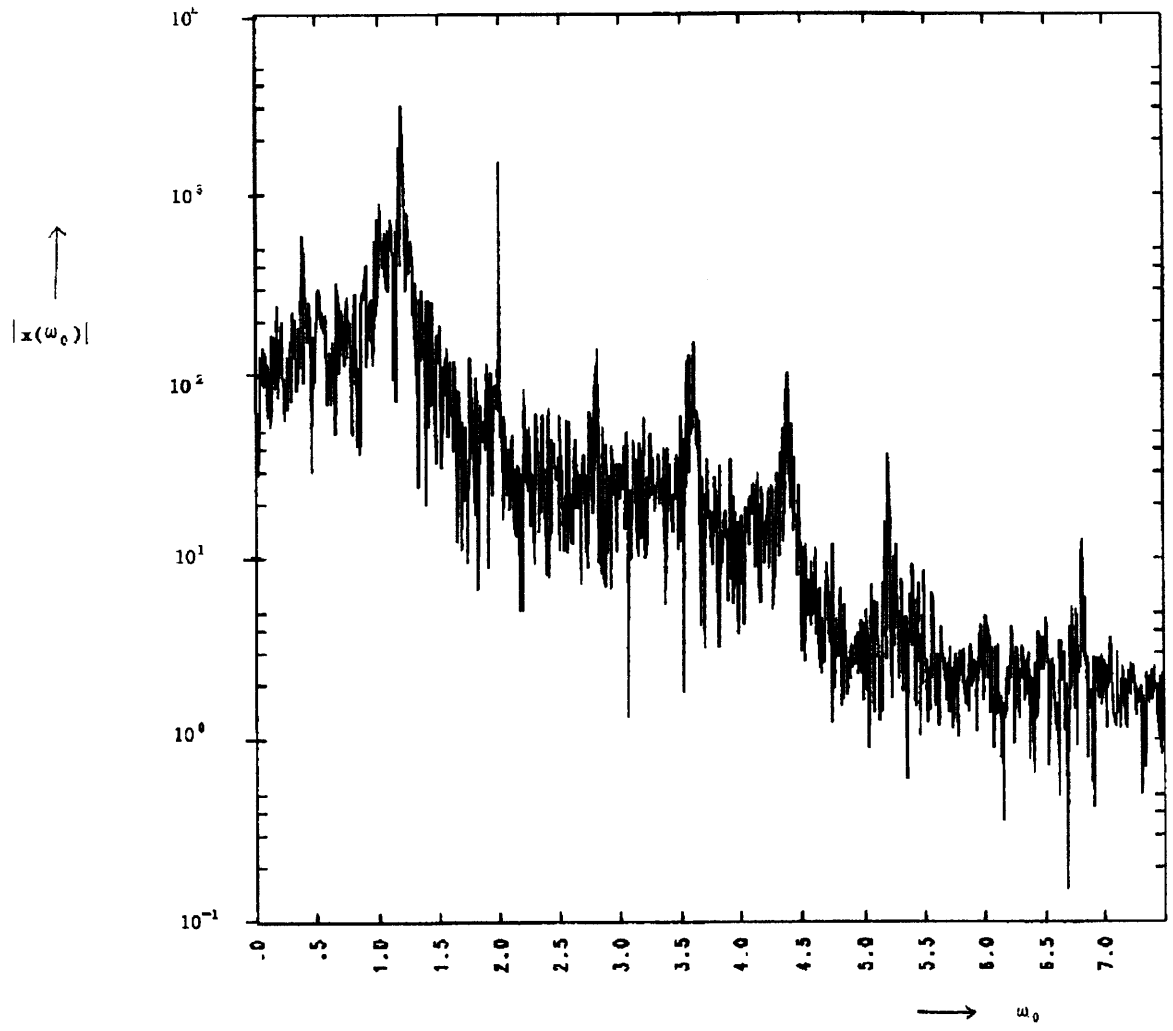

Figure 7. The frequency spectrum of x for the chaotic case ($\varepsilon = 0.79$).

force-free state) when, under certain conditions, they oscillate at the frequency of the drive. Self-oscillatory systems are linearly unstable so that the initial amplitude of the oscillations grows in time. The amplitude eventually saturates due to nonlinearities, leading to the self-oscillation steady-state.[30]

We have been studying the behavior of a self-oscillating system when acted upon by a temporally oscillating force. The model we are studying combines a van der Pol-type of self-oscillating nonlinearity with a Duffing-type of nonlinear potential. The governing equation of motion is of the form:

$$\frac{d^2x}{dt^2} - \mu(1 - \gamma x^2)\frac{dx}{dt} + \alpha x + \beta x^3 = \varepsilon \cos \omega t \quad (1)$$

where the right-hand side is the external drive. For $\mu < 0$, $\gamma = 0$, $\alpha < 0$, and $\beta > 0$, the left-hand side describes the Duffing oscillator, while for $\mu > 0$, $\gamma > 0$, $\alpha > 0$, and $\beta = 0$, it describes the van der Pol oscillator. The van der Pol oscillator is self-oscillatory

[30] Ibid.

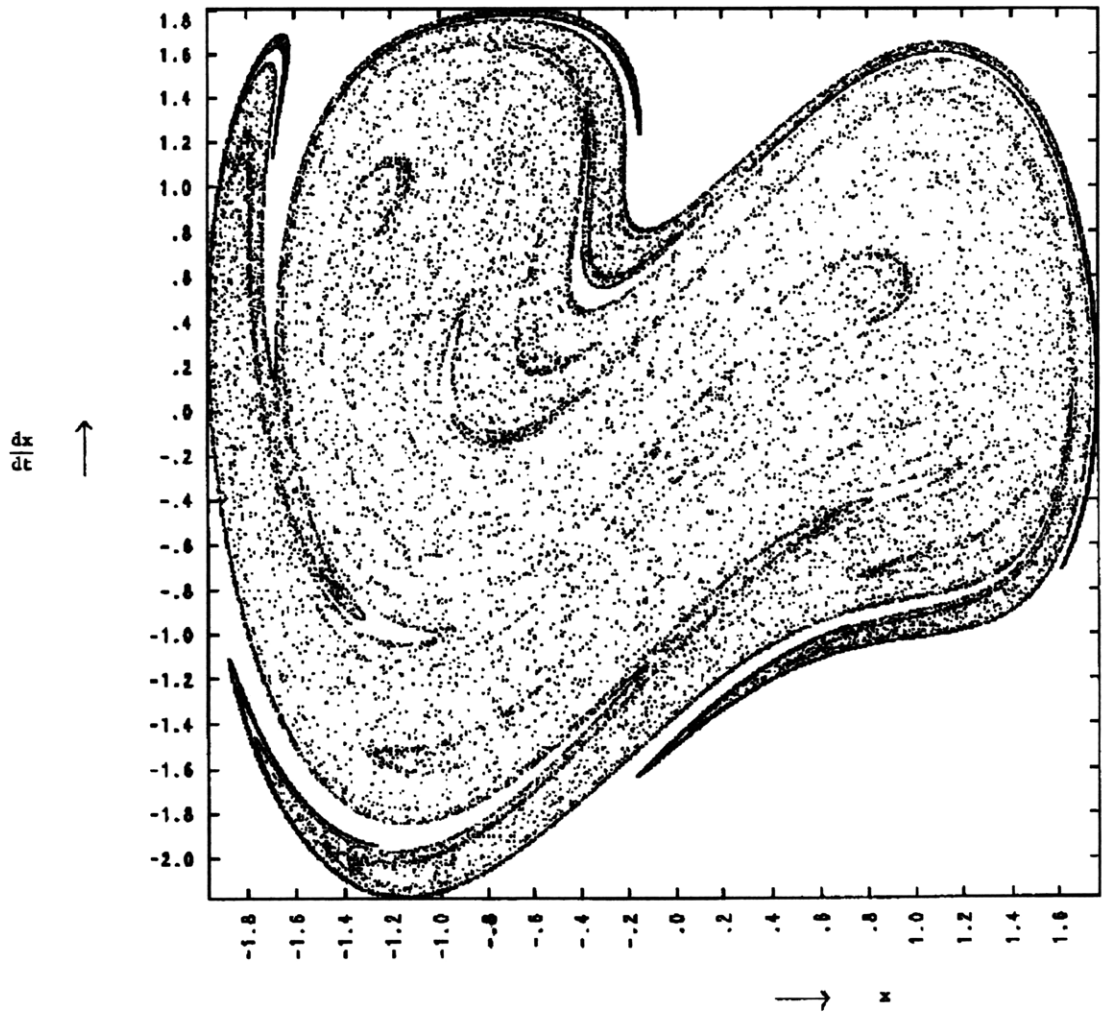

Figure 8. The Poincaré surface of section showing the strange attractor for the chaotic case ($\varepsilon = 0.79$).

(unlike the Duffing oscillator) and exhibits frequency locking as well as quasiperiodicity under the influence of an external drive.[31] However, we found, through our numerical investigations, that the van der Pol oscillator, within the range of parameters we investigated, does not behave chaotically.[32] After investigating the case in which $\alpha = 0, \beta > 0$, corresponding to a van der Pol oscillator with a nonlinear restoring force, we found that it leads to chaos for very large values of ε and for ω much larger than the natural frequency of self-oscillations of the system.[33] Meanwhile, it is well-known that the Duffing oscillator exhibits chaotic motion when

[31] Ibid.

[32] Y. Ueda and N. Adamatsu, "Chaotically Transitional Phenomena in the Forced Negative-Resistance Oscillator," *IEEE Trans. Circuits Syst.* CAS-28: 217-224 (1981).

[33] C. Hayashi, *Nonlinear Oscillations in Physical Systems* (New York: McGraw Hill Book Co., 1964); Y. Ueda and N. Adamatsu, *IEEE Trans. Circuits Syst.* CAS-28: 217-224 (1981).

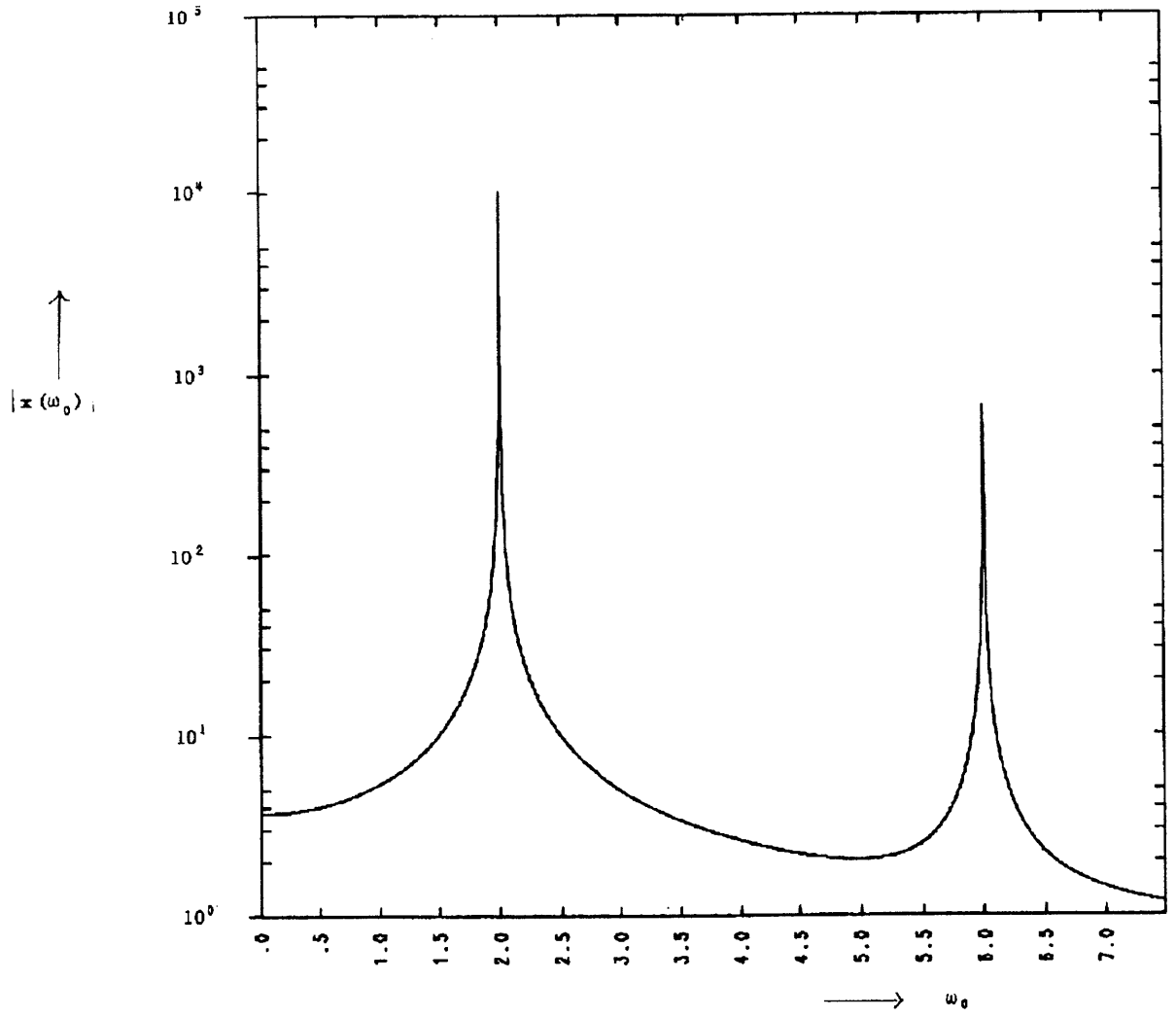

Figure 9. The frequency spectrum of x for the frequency locked case ($\varepsilon = 1.94$).

driven by external periodic force.[34] Upon combining the van der Pol self-oscillating nonlinearity with the Duffing potential equation (1), we found that the system became chaotic for small values of ε and for ω close to the natural frequency of self-oscillations.

The system which we studied was with $\mu > 0$, $\gamma > 0$, $\alpha < 0$, and $\beta > 0$. The frequency of self-oscillations, Ω, of the (stable) limit cycle of the system is (to leading order in μ) given by $\Omega^2 = |\alpha| + (3\beta/\gamma)$. The amplitude, A of the limit cycle (to the same order in μ) is: $A^2 = 4/\gamma$. With an imposed external force this system exhibits a very rich dynamical behavior encompassing a variety of nonlinear dynamics phenomena. As a function of ε and ω, the system demonstrates periodic, quasiperiodic, frequency locked, and chaotic states.

We have numerically solved equation (1) for $\mu = 0.4$, $\alpha = -1$, $\beta = 1$, $\gamma = 1$, $\omega = 2$ and as

[34] Y. Ueda, "Steady Motions Exhibited by Duffing's Equation: A Picture Book of Regular and Chaotic Motions," in *New Approaches to Nonlinear Problems in Dynamics,* ed. P.J. Holmes (Philadelphia: SIAM, 1980).

a function of ε. For those parameters, the frequency of the limit cycle ($\varepsilon = 0$) is $\Omega \approx 1.13$. As ε is increased, the system has quasiperiodic solutions, shown in figure 6. The transition to chaos occurs around $\varepsilon \sim 0.785$. Figures 7 and 8, respectively, show the frequency spectrum and the strange attractor for $\varepsilon = .79$, where the system is chaotic. The transition to frequency locking, where the system (1) oscillates at the driving frequency (ω), occurs around $\varepsilon \sim 1.93$ (see figure 9). The transition to locking is abrupt (e.g., at $\varepsilon = 1.9322$ the system is chaotic, while at $\varepsilon = 1.9323$ the system is locked). Before reaching this frequency locked state, the system goes through other regions of locking where the ratio of the frequency of the system to ω is a rational number.

The system behaves similarly for fixed ε and as a function of ω. For $\varepsilon = 1$ and $\omega \sim \Omega$, there is frequency locking. As ω is increased, there is a transition to chaos around $\omega \sim 1.8$. The transition to quasi-periodicity occurs around $\omega \sim 2.3$.

Publications

Batchelor, D.B., E.F. Jaeger, B.A. Carreras, H. Weitzner, K. Imre, D.C. Stevens, V. Fuchs, and A. Bers. "Full-Wave Modeling of Ion-Cyclotron Heating in Tokamaks." Proceedings of the 12th International Atomic Energy Agency Conference on Plasma Physics and Controlled Nuclear Fusion, Nice, France, October 12-19, 1988, Vol. 1, 611-620, IAEA-CN-50/E-II-5. Vienna: International Atomic Energy Agency, 1989.

Bers, A., G.S. Triantafyllou, and A.K. Ram. "Absolute Instabilities in Inhomogeneous Flows." *Bull. Am. Phys. Soc.* 34: 2263 (1989).

Chow, C., A. Bers, and V. Fuchs. "Analytic Studies of ICRF Heating." In *Radio Frequency Power in Plasmas.* A.I.P. Conf. Proc. 190. Ed. R. McWilliams, 234-237. New York: American Institute for Physics, 1989.

Chow, C., V. Fuchs, and A. Bers. "Reflection at the Resonance Layer of the Fast Alfvén Wave in Ion Cyclotron Heating." Submitted to *Phys. Fluids B.*

Chow, C., V. Fuchs, and A. Bers. "The Dispersion Relation for D(^{3}He) Ion-Cyclotron Resonance Heating." *Phys. Fluids B.* Forthcoming.

Chow, C., V. Fuchs, and A. Bers. *Reflection at the Resonance Layer of the Fast Alfvén Wave in Ion Cyclotron Heating.* MIT Plasma Fusion Center Report PFC/JA-90-2. Cambridge: MIT, 1990.

Chow, C., V. Fuchs, and A. Bers. *The ICRF Dispersion Relation for* D(^{3}He). MIT Plasma Fusion Center Report PFC/JA-89-42. Cambridge: MIT, 1989.

Chow, C., V. Fuchs, and A. Bers. "An Analytic Theory of ICRF Heating." (Abstract) *Bull. Am. Phys. Soc.* 34: 2094 (1989).

Chow, C., V. Fuchs, and A. Bers. "Analytic Studies of ICRF Heating." Paper presented at the Sherwood Theory Conference, San Antonio, Texas, April 3-5, 1989.

Chow, C., A. K. Ram, and A. Bers. "Damping of the Fast Alfvén Wave in Ion-Cyclotron Resonance Heating." *Phys. Fluids B* 1(10):2018-2026 (1989).

Chow, C., A.K. Ram, and A. Bers. *Damping of the Fast Alfvén Wave in Ion-Cyclotron Resonance Heating.* MIT Plasma Fusion Center Report PFC/JA-89-19. Cambridge: MIT, 1989.

Kupfer, K., A. Bers, and A.K. Ram. "Guiding Center Stochasticity by Electrostatic Waves in Toroidal Geometry." (Abstract) *Bull. Am. Phys.* Soc. 34: 1927 (1989).

Kupfer, K., A. Bers, and A.K. Ram. "RF Induced Transport in Tokamak Plasmas." In *Radio Frequency Power in Plasmas.* A.I.P. Conf. Proc. 190, ed. R. McWilliams, 434-437. New York: American Institute for Physics, 1989.

Kupfer, K., A. Bers, and A.K. Ram. "Transport of Charged Particles Interacting with Coherent Wave-Fields in a Tokamak

Plasma." Paper presented at the Sherwood Theory Conference, San Antonio, Texas, April 3-5, 1989.

Kupfer, K., A. Bers, and A.K. Ram. "Transport of Charged Particles Interacting with Coherent Wave-Fields in a Tokamak." Abstract presented at the Transport Task Force Meeting, Institute for Fusion Studies, Austin, Texas, January 11-13 1989.

Ram, A.K., and A. Bers. "Ray Tracing of Mode-Converted Ion-Bernstein Waves in Toroidal Plasmas." Paper presented at the Sherwood Theory Conference, San Antonio, Texas, April 3-5, 1989.

Ram, A.K., and A. Bers. "Kinetic Ray Tracing in Toroidal Geometry with Application to Mode-Converted Ion-Bernstein Waves." In *Proceedings of the 1989 International Conference on Plasma Physics,* New Delhi, India, 57-60. Eds. A. Sen and P.K. Kaw, 1989.

Ram, A.K., and A. Bers. "Kinetic Ray Tracing in Toroidal Plasmas." (Abstract) *Bull. Am. Phys. Soc.* 34: 2094 (1989).

Ram, A.K., and A. Bers. *Kinetic Ray Tracing in Toroidal Geometry with Application to Mode-Converted Ion-Bernstein Waves.*. MIT Plasma Fusion Center Report PFC/JA-89-37. Cambridge: MIT, 1989.

Ram, A.K., A. Bers, and K. Kupfer. "Periodic Interactions of Charged Particles with Spatially Localized Fields." *Phys. Lett.* A 138: 288-294 (1989).

Shoucri, M., I. Shkarofsky, V. Fuchs, K. Kupfer, A. Bers, and S. Luckhardt. "A Quasilinear Fokker-Planck Code for the Numerical Solution of the Lower-Hybrid Current Drive Problem in the Presence of Electron Cyclotron Heating." *Comp. Phys. Comm.* 55: 253-268 (1989).

Shoucri, M., I. Shkarofsky, V. Fuchs, K. Kupfer, A. Bers, and S. Luckhardt. *A Quasilinear Fokker-Planck Code for the Numerical Solution of the Lower-Hybrid Current Drive Problem in the Presence of Electron Cyclotron Heating.* Report No. CCFM-RI-298e. Varennes, Canada: Centre Canadien de Fusion Magnetique, Tokamak de Varennes, 1989.

1.3 Physics of Thermonuclear Plasmas

Sponsor

U.S. Department of Energy
Contract DE-AC02-ET-51013

Project Staff

Professor Bruno Coppi, Dr. Ronald C. Englade, Dr. Stefano Migliuolo, Dr. Linda E. Sugiyama, Sergio Angelini, Riccardo Betti, Paolo Detragiache, Darin Ehrnst, Marco Nassi

The main theme of our research program is the theoretical study of magnetically confined plasmas in regimes of thermonuclear interest. A variety of physical regimes that fall in this category characterize both present-day experiments on toroidal plasmas (e.g., Alcator, TFTR, JET) as well as future experiments that will contain ignited plasmas. These will either involve first generation fuels, namely a deuterium-tritium mixture (Ignitor, CIT), or more advanced fuels such as deuterium-deuterium or deuterium-helium mixtures (Candor).

We are participating in a collaborative effort involving the U.S. design group for the compact ignition experiment (CIT) and that for the European experiment, Ignitor. At MIT, the Alcator C-MOD experiment, combining the favorable features of elongated plasma cross section with high magnetic field, is under construction. These features, which are also being planned for CIT and Ignitor, were originally proposed for a machine called Megator, which we designed in the early 1970s.

Presently, our research program follows two major avenues. First, we are studying the basic physical processes of thermonuclear plasmas (equilibrium, stability, transport, etc.) as applied to existing or near-term future systems. In this effort, we are collaborating closely with our experimental colleagues, as well as with theorists from other research groups (e.g., JET, Princeton, Columbia). This work also involves time-

dependent simulations of plasma discharges in the planned D-T burning Ignitor experiment, with particular attention being focused on the evolution of spatial profiles of plasma current and temperature. Collaboration with our colleagues at the Italian laboratories of E.N.E.A., as well as in-house code development by a young scientist "on loan" from Italy plays a major role in this endeavor. Second, we are exploring advanced regimes of thermonuclear burning, including those employing low neutron yield fuels (D-^{3}He, and "catalyzed" D-D). We are considering the design of machines that will contain these very high temperature plasmas as well as the physics that govern their behavior.

In the following section, we present some of the salient results of work which members of our research group have completed or are presently involved with.

1.3.1 Symmetries and Global Transport Equations

Understanding the time evolution of the current density profile and of the electron temperature is necessary in order to assess the effectiveness of the ohmic heating and, in general, to predict the stability of the plasma against global (resistive) MHD modes whose excitation depends on the current density distribution.

We formulate[35] constraints that apply to the current density profile in a high temperature toroidal plasma and introduce an effective thermal force and electron viscosity term in the current density equation. Correspondingly, the electron thermal energy equation acquires new terms. A matrix equation that relates the electron thermal energy transport to that of the current density is derived. The symmetry properties of this matrix are identified and used to prescribe realistic conditions on the electron temperature and current density profiles.[36]

These profiles are relevant to high temperature regimes where: (a) the presence of a population of magnetically trapped electrons affects the plasma resistivity in such a way as to cause a current density distribution with a cusp-like profile[37] at the magnetic axis for the observed (canonical)[38] electron temperature profiles, when a simple Ohm's law is adopted to relate the current to the electric field, (b) the "ballooning" character of the m=1, n=1 instability which is driven by the plasma pressure gradient and can be expected to lead mainly to a pressure profile relaxation, leaving the current density profile mostly unchanged.

Furthermore, as the plasma temperature is increased, the contribution to the stability of this mode by terms related to microscopic plasma properties becomes important. In an ignited plasma, the presence of a population of energetic particles may lead to regimes where the m=1, n=1 relaxation is suppressed. These effects are not expected to account for the m=1, n=2 instability so that one half can be taken as a "hard" lower bound for the (inverse) helicity parameter, i.e., $q_0 > 1/2$.

1.3.2 Stabilization of Drift-Tearing Modes

A region of stability, in $\omega_{*e}\tau_H - \Delta'$ parameter space (where $\omega_{*e} = (mc/eBrn)(dp_e/dr)$ = electron diamagnetic frequency, m = poloidal mode number, τ_H = characteristic hydrodynamic time, Δ' = stability parameter for tearing modes) is discussed.[39] The growth rate of the drift-tearing mode is found to be a non-monotonic function of Δ'. As Δ'

---

[35] B. Coppi and F. Pegoraro, MIT/RLE Report PTP-90/2, MIT, 1990.

[36] Ibid.

[37] B. Coppi and L. Sugiyama, *Comm. Plasma Phys. Cont. Fusion* 10:43 (1986).

[38] B. Coppi, *Comm. Plasma Phys. Cont. Fusion* 5:261 (1980).

[39] S. Migliuolo, F. Pegoraro, and F. Porcelli, submitted to *Phys. Fluids* (1990).

increases from zero, the growth rate first reaches a maximum for $\Delta' \approx 0.5\Delta'_1$ and becomes negative for $\Delta' \geq \Delta'_1 \approx 2m/\sqrt{\tau_H \omega_{*e}(\omega_{*e} - \omega_{*i})}$. Here ω_{*i} is the corresponding ion diamagnetic frequency. As this threshold for restabilization is approached, the mode eigenfrequency, ω moves further and further away from ω_{*e}, and the mode eigenfunction acquires a strongly varying form within the singular layer. This is recognized as the breakdown of the constant-Ψ approximation, which occurs[40] in conjunction with large parallel electron currents within the layer, shielding of the perturbation from the ideal region and inhibiting reconnection.

As Δ' is increased further past a second threshold value $\Delta'_2 \approx \sqrt{2\tau_H \omega_{*e}/\varepsilon_\eta}$ (where $\varepsilon_\eta = \eta c^2 \tau_H / 4\pi r_0^2$ is a measure of the collisional resistivity at the singular surface, $q(r = r_0) = 1$), a second root becomes unstable. This root corresponds to the diamagnetic modification of the $\varepsilon_\eta^{1/3}$ version of the resistive tearing mode. For the m=1 case this mode is known as the resistive internal kink. Its stabilization for $\Delta' \leq \Delta'_2$, is understood to arise from the lessening in the free energy available to the mode from the plasma pressure gradient.

This window of stability had been identified previously,[41] but its large width had been hitherto unrecognized. Its primary dependence is on ω_{*e}, with a weak dependence on the electron-ion temperature ratio: it disappears entirely for $\omega_{*e}\tau_H \leq 0.83\varepsilon_\eta^{1/3}$. In figure 10, we show the stability diagram in the $\omega_{*e} - \Delta'$ space. The heavy continuous line denotes marginal stability, $\mathrm{Im}(\omega) = 0$, while regimes are shown in which various modes appear with characteristic growth rates: $\gamma_R = m^{2/3}\varepsilon_\eta^{1/3}\tau_H$ is the basic resistive mode growth rate, $\gamma_R^* = m^2\varepsilon_\eta / |\omega_{*e}\omega_{*i}|\tau_H^3$ is the growth rate modified by finite diamagnetic frequency, $\gamma_T \approx 0.5 m^{2/5}\varepsilon_\eta^{3/5}(\Delta')^{4/5}/\tau_H$ is that of the tearing mode, and $\gamma_{DT} \approx 0.2 m^{2/3}\varepsilon_\eta(\Delta')^{4/3}[\omega_{*e}(\omega_{*e} - \omega_{*i})]^{-1/3}\tau_H^{-5/3}$ is that of the drift-tearing mode. There exists a branch cut for the problem, arising from the dispersion relation which can be written as:[42]

$$\Delta'\delta = \frac{-m\pi}{8} Q \frac{\Gamma[(Q-1)/4]}{\Gamma[(Q+5)/4]}$$

where $\delta^4 \equiv -im^2\varepsilon_\eta\tau_H\omega(\omega - \omega_{*i})/(\omega - \omega_{*e})$, and $Q \equiv -i\delta^2(\omega - \omega_{*e})/\tau_H m^2 \varepsilon_\eta$. Following one root of the dispersion relation along a closed path that encirles this point will cause us to return to the point of departure with a different eigenfrequency than that with which we started.

This theory applies directly to resistive m=1, n=1 modes with the substitution $\Delta' \rightarrow -m\pi/\lambda_H$. Values of parameters that correspond to the stable domain in figure 10 are relevant to m=1 modes in magnetically confined toroidal plasmas with low values of the poloidal beta parameter. For these modes, the stable region can be accessed when the magnetic shear, $\hat{s}$, is reduced near the q=1 surface even if q at center is significantly less than unity. This is because $\tau_H\omega_{*e}/\varepsilon_\eta^{1/3} \propto \hat{s}^{-2/3}$, while $\hat{\lambda}_H = -\pi m^{1/3}/(\Delta'\varepsilon_\eta^{1/3}) \propto (q_0 - 1)/\hat{s}^{5/3}$.[43] Thus, lowering the shear takes us toward the upper left corner of figure 10, i.e., deep into the stable region.

1.3.3 $M^0 = 1$ Internal Modes in High Temperature Regimes

As present experiments (e.g., JET) reach the multi-keV regime of plasma temperatures, models for the stability of $m^0 = 1$ internal modes must be improved to account for kinetic effects due to the ions and electrons. In these regimes, as well as in those relevant

---

[40] J.F. Drake, T.M. Antonsen, Jr., A.B. Hassam, and N.T. Gladd, *Phys. Fluids* 26:2509 (1983).

[41] M.N. Bussac, R. Pellat, D. Edery, and J.L. Soule, in *Plasma Physics and Controlled Nuclear Fusion Research 1976* (Vienna:IAEA, 1977), Vol. 1, p. 607; B. Coppi, R. Englade, S. Migliuolo, F. Porcelli, and L. Sugiyama, in *Plasma Physics and Controlled Nuclear Fusion Research 1986* (Vienna: IAEA, 1987), Vol. 3, p. 397.

[42] S. Migliuolo, F. Pegoraro, and F. Porcelli, submitted to *Phys. Fluids* (1990).

[43] F. Porcelli, W. Han, F. Pegoraro, and A. Taroni, *JET Report JET-IR(88)16.*

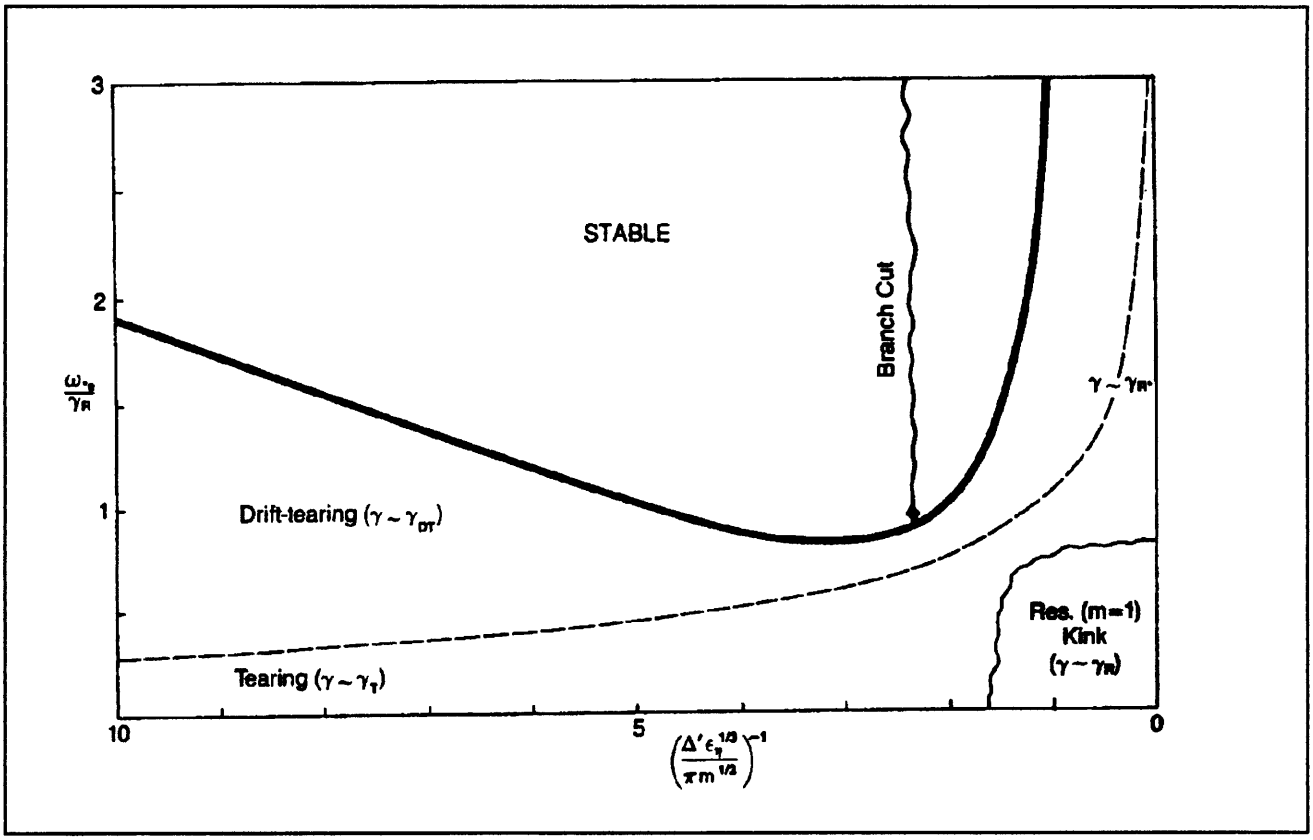

Figure 10. Stability diagram for resistive internal modes and drift-tearing modes. For $m^0 = 1$, $\Delta'/m\pi \rightarrow -1/\lambda_H$.

to planned ignition experiments such as Ignitor, standard two-fluid theory[44] is inadequate: the gyral radius of the plasma ions, ρ_i, becomes a finite fraction of the scaled radius of the singular surface, $\varepsilon_\eta^{1/3} r_0$. Here r_0 is the radius where $q(r) = rB_\zeta/RB_\theta = 1$ and $\varepsilon_\eta = \eta c^2 \tau_H / 4\pi r_0^2$ is a measure of the electrical resistivity. As a consequence finite Larmor radius (FLR) effects must be taken into account. These effects are known[45] to be destabilizing because they establish a minimum value for the thickness of the singular layer about $r = r_0$, where reconnection can occur: $\delta/r_0 = \max(\rho_i/r_0, \lambda_H)$ where λ_H is the ideal MHD stability parameter. Also, in regimes where $\lambda_H < \rho_i/r_0$, FLR acts to raise the mode frequency thereby lessening the stabilizing effect of finite diamagnetic ion frequency (ω_{*i}).

We have generalized the kinetic model described in Pegoraro et al.,[46] including the stabilizing effects of ion viscosity through a particle and momentum conserving Krook collision operator. For low values of FLR and ion viscosity effects (i.e., compared to λ_H and in the regime where the ideal mode is stable, $\lambda_H < \omega_{*i}\tau_H/2$), the normalized eigenfrequency of the internal $m^0 = 1$ resistive kink, $\lambda = -i\omega\tau_H$ becomes:

$$\lambda = i\frac{\lambda_H^2}{\lambda_i} + \frac{5\varepsilon_\eta}{2\lambda_i^2} - \frac{\rho_i^2 \lambda_v}{4\lambda_H^2}$$

---

[44] G. Ara, B. Basu, B. Coppi, G. Laval, M.N. Rosenbluth, and B.V. Waddell, *Ann. Phys. (N.Y.)* 112:443 (1978).

[45] F. Pegoraro, F. Porcelli, and J.J. Schep, *Phys. Fluids* B1:364 (1989).

[46] Ibid.

$$\left[\frac{\lambda_i^2\lambda_\nu^2 + 2\lambda_H^4}{\lambda_i^2\lambda_\nu^2 + \lambda_h^4 - \frac{3}{4}} \right]$$

$$+ \frac{i\rho_i^2}{4\lambda_i} \left[\frac{3}{4} - \frac{\lambda_i^2\lambda_\nu^2}{\lambda_i^2\lambda_\nu^2 + \lambda_H^4} \right]$$

which clearly shows the stabilization of the FLR enhanced resistive mode when $\lambda_\nu \equiv \nu_i\tau_H$ is large enough to overcome the effect of finite electrical resistivity, e.g., $\lambda_\nu \geq 40\varepsilon_\eta(\lambda_H/\rho_i\lambda_i)^2$ when $\lambda_H^4 \ll \lambda_i^2\lambda_\nu^2$.

We are continuing this study by numerically exploring regions in parameter space (e.g., $\lambda_H \to 0$ and/or $\rho_i/\varepsilon_\eta^{1/3}r_0 > 1$) where analytic perturbation techniques are inappropriate. In this manner, we are able to rather accurately predict regimes where ignition experiments (e.g., Ignitor) will be able to operate without incurring sawtooth crashes.

1.3.4 Nonlinear Ballooning Modes

Ballooning modes[47] play a very important role in the dynamics of high β equilibrium configuration. A two dimensional Rayleigh-Taylor-ballooning-like model has been developed to simulate their nonlinear behavior. In this model the equilibrium magnetic field lines are at an angle ψ with the two-dimensional domain. Two forces act on the plasma: the buoyancy force which drives the dense fluid to the bottom and the less dense fluid to the top; and the line bending force, which resists any movement of the fluid and vanishes at ψ = 90 deg.

A set of reduced MHD equations,[48] is numerically solved using a novel magnetic stress-tensor formulation,[49] which allows energy conservation with an explicit time advance, and a finite difference scheme in both directions.

An equilibrium configuration with a steep density gradient has been studied extensively in both the ideal and resistive regimes, and for different initial perturbations.

In the ideal case with random initial conditions, the dominant mode chooses a wavelength that is the maximum between the grid size and $\hat{K}y^2d^2 = (1/v_A^2)(gd/r_\rho)/\sin^2\Phi - \pi/2$ where d is the vertical dimension, v_A is the Alfvén speed, g is the gravity, r_ρ is the density gradient scale length, and $\Phi = \pi/2 - \phi$. The saturation mechanism is provided by the bending of the magnetic field lines. Single wavelength initial perturbations have shown a non-linear growth of a bubble-like structure in the limit of a very steep density gradient and large value of the angle ψ.

The inclusion of resistivity[50] drives unstable modes with wavelengths of the size of the physical domain in the presence of perfect conducting walls and incompressible flow.

The numerical solution is in good agreement with the finite amplitude analytic results obtained with a multiple time scale anlaysis of the equations for a sharp boundary configuration and an angle $\psi = 0$.[51]

In order to include the effect of magnetic field curvature as the driving mechanism, a three-dimensional code is being developed. A preliminary simplified version of the code has been completed using finite difference in all three dimensions and the first results were

---

47 B. Coppi, J. Filreis, and F. Pegoraro, *Ann. Phys.* 121:1 (1979).

48 H.R. Strauss, *Phys. Fluids* 8:1354 (1977).

49 R. Betti, J.U. Brackbill, B. Coppi, and J.P. Freidberg, *Proceedings of the 13th Plasma Simulation Conference,* Santa Fe, New Mexico, 1989.

50 H.P. Furth, J. Killeen, M.N. Rosenbluth, and B. Coppi, in *Plasma Physics and Controlled Nuclear Fusion Research 1966* (Vienna: IAEA, 1967), Vol. 1, p. 103; B. Coppi, *Phys. Rev. Lett.* 39:939 (1977).

51 R. Betti, J.U. Brackbill, B. Coppi, and J.P. Freidberg, *Bull. Am. Phys. Soc.* 34:2046 (1989).

reported at the 1989 APS meeting.[52] However, the final version of the three-dimensional mode will adopt spectral method in θ and ϕ,[53] finite difference in r, and a Semi-Implicit time advance algorithm.[54]

1.3.5 SOL Plasma Behavior in a Compact High Field Torus

Recent data for large and small limiter tokamaks in the ohmic phase have been analyzed. These experimental results have been correlated[55] to important properties of the plasma scrape-off layer (SOL), namely: $\nabla_{\parallel} T_e \neq 0$, plasma recycling, shielding of impurities, and radiative cooling. The basic behavior of the SOL plasma in the Ignitor device may be anticipated on the basis of simple physical considerations.[56] Recent experimental data has confirmed that the higher the average density is, the lower are the edge temperature and edge density.[57] A high edge density means a high probability of interaction between ions and neutrals as well as impurities. Taking into account that the average density predicted in the Ignitor device is an order of magnitude larger than that in present large tokamaks, the following phenomena may be expected:

- High ionization rate of neutrals, hence a high level of recycling.
- Ability to screen the main plasma from impurities and, thus, the opportunity to reduce Z_{eff}.
- High level of impurities in the SOL plasma and its strong radiative cooling.

The main numerical results[58] have been obtained for plasma edge density $= 2.4 \times 10^{20}$ m^{-3} (with $\bar{n} = 6 \times 10^{20}$m^{-3}), edge temperature = 10 eV, and scrape-off decay length = 7.5×10^{-3} m. These results confirm that the SOL in the Ignitor device has a complex behavior and that some distributed processes ($\nabla_{\parallel} T_e$, recycling, impurity shielding, radiative cooling) are occurring. The consequences of this situation for the power balance and for the thermal wall loading can be summarized as follows:

- The radiative cooling becomes dominant.
- The mean kinetic energy of the ions impinging on the first wall is low (4.8 eV) and might be lower than that required to cause sputtering.
- The thermal wall loading is of the order of 1.2 MW/m^2.

1.3.6 Plasma Dynamics Simulation by the TSC Code

We have begun an investigation of the plasma dynamics of the flat top of the plasma current, as well as of the ramp-up phase, of the discharge in a deuterium-tritium ignition experiment, using the TSC[59] code. This Tokamak Simulation Code, developed at PPPL, models the axisymmetric transport time evolution, positional stability, and control properties of non-circular, free

---

[52] Ibid.

[53] H.C. Ku, R.S. Hirsh, and T.D. Taylor, *J. Comp. Phys.* 70 (1987).

[54] D.D. Schnack, D.C. Barnes, and Z. Mikic, *J. Comp. Phys.* 70 (1987).

[55] P.C. Strangeby, *J. Nucl. Mat.* 105:145-147 (1987).

[56] P.C. Strangeby, in *Physics of Plasma Wall Interactions in Controlled Fusion,* eds. D.E. Post and R. Behrisch (New York: Plenum Press, 1986); J. Roth, ibid.; P.C. Strangeby, *Phys. Fluids* 28:55 (1985).

[57] S.K. Erents et al., *Nucl. Fusion* 28:1209 (1988).

[58] M. Nassi, in *Tritium and Advanced Fuels in Fusion Reactors,* ISPP-5, eds. G. Bonizzoni and E. Sindoni (Bologna, Italy: SIF, 1989), p. 289.

[59] S.C. Jardin, N. Pomphrey, and J. DeLucia, *J. Comp. Phys* 66: 481 (1986).

boundary tokamaks.[60] It provides a time dependent, nonlinear description of the axisymmetric MHD and transport behavior of the plasma in two spatial dimensions. This problem is very complex, due to the disparate time scales of diffusion-like and wave-like phenomena, and to the anisotropy introduced by the magnetic field. A self-consistent solution is obtained by solving the plasma momentum and field evolution equations on a two-dimensional X-Z grid, and the plasma energy and particle evolution equations in a one dimensional coordinate system which evolves with the plasma magnetic surfaces.[61] The TSC code takes into account the plasma interaction with a set of poloidal conductors that model the passive structure of the plasma chamber as well as with the active poloidal field coils. These conductors obey electromagnetic circuit equations with active feedback systems included.

An extensive numerical simulation is being performed in order to determine the characteristic time scale for vertical instability of the plasma column and to design a feedback system to control it. The axisymmetric vertical instability occurs when the plasma column shifts rapidly due to a loss of vertical control. As soon as the plasma moves slightly off the equilibrium position at the midplane, its current interacts with the radial component of the external poloidal magnetic field, giving rise to a force that increases its vertical displacement. This motion, if not controlled, leads to a disruption. The rapid plasma displacement from the midplane induces toroidal currents in the upper and lower halves of the vacuum vessel, which flow in opposite directions. These currents interact with the plasma and produce a force that attempts to return the column back to its equilibrium position. This stabilizing effect is very important because it increases the time scale for the vertical instability from an ideal MHD time measured in microseconds to the L/R time scale (milliseconds). On this slower time scale, it is possible to design an active feedback system which can control the plasma vertical position. Preliminary results have been presented[62] on the growth rate of the plasma vertical instability with and without an external stabilizing structure and on the plasma vertical position control by an external feedback system.

Preliminary results[63] on the ignition plasma performance using the Coppi-Tang transport model[64] as well as a study on the Volt-second requirements throughout the discharge have been presented.[65] We have modified the transport model by assuming that the anomalous electron heat flux can be described by a modified form of the Coppi-Mazzucato-Grüber thermal diffusivity, which can reproduce ohmic and L- or H-mode experimental results in the auxiliary heating regimes. We are presently engaged in studying the problem of the plasma current penetration during the current ramp phase of the discharge in which the magnetic field, current, and plasma density are simultaneously ramped.

1.3.7 Thermal Transport in the Transition Regime

We have used a transport code to investigate semi-empirical forms for anomalous electron and ion heat transport in the transition regime linking "cool" ohmic plasmas and "hot" discharges sustained predominantly by

---

[60] S.C. Jardin et al., *Nucl. Fusion* 27: 569 (1987); B.J. Merril and S.C. Jardin, *J. Nucl. Mat.* 881: 145-147 (1987).

[61] S.C. Jardin, in *Multiple Time Scale,* eds. J.U. Brackbill and B.I. Cohen (New York: Academic Press, 1985).

[62] M. Nassi, in *Tritium and Advanced Fuels in Fusion Reactors,* ISPP-5, eds. G. Bonizzoni and E. Sindoni (Bologna, Italy: SIF, 1989), p. 289.

[63] M. Nassi, S.C. Jardin, and N. Pomphrey, *Bull. Am. Phys. Soc.* 34: 1974 (1989).

[64] W.M. Tang, *Nucl. Fusion* 26: 1605 (1986).

[65] M. Nassi, in *Tritium and Advanced Fuels in Fusion Reactors,* ISPP-5, eds. G. Bonizzoni and E. Sindoni (Bologna, Italy: SIF, 1989), p. 289.

external auxilary heating or fusion heating.[66] Knowledge of the thermal transport appropriate to this regime is particularly relevant to the expected performance of compact ignition devices such as Ignitor and CIT.

We have represented the electron heat diffusivity with a modified form of the well-known Coppi-Mazzucato-Grüber coefficient, written as:

$$\chi^e = \frac{7.9 \times 10^{15}}{\bar{A}_i^{0.4} n_e} \frac{I(r)}{T_e(r)} \frac{a}{r^2}$$

$$\left[1 + \gamma_0 \left(1 - \frac{P_{OH}}{P_{TOT}} \right)^2 <\beta_p> \right]$$

where I is the total plasma current in kA within the radius r, n_e is the electron density in cm^{-3}, T_e is the electron temperature in keV, a is the radius of the outermost flux surface in cm, $\bar{A}_i$ is the mean ion atomic weight, P_{OH} and P_{TOT} are the Ohmic and total heating powers, and $<\beta_p>$ is the volume average total poloidal beta parameter.

This transport accounts reasonably well for the temperature behavior of a wide variety of ohmically heated toroidal devices when the effects of ion heat conductivity are small. The term proportional to $<\beta_p>$ is intended to reflect an enhanced level of microinstabilities that accompanies the increase of the thermal energy content above a threshold value assumed close to that of a steady state ohmic discharge.[67] The ion heat transport is modelled with a combination of neoclassical and anamolous thermal diffusivity. For operational purposes, we assume the latter to have the same outwardly increasing spatial behavior as the χ_e discussed above but with a magnitude that is allowed to vary from simulation to simulation.

We have applied this model to a series of ohmic and L-mode neutral beam heated discharges performed at 1.4 MA and 2.2 MA on the TFTR device in which the individual temperature behavior of the electrons and ions could be resolved.[68] Comparing simulation results with the observations and directly testing the effects of model variation, we find that $\gamma_0 \simeq 9.0$ in combination with a ratio of $(\chi_i/\chi_e)^{ANOM}$ that increases with auxiliary power from 0.2 at $P_{AUX} = 0$ ($T_i \sim 2.5$ keV) to a value between 1.1 and 1.8 at $P_{AUX} = 15$ MW ($T_i \sim 8$ keV) yields a good fit for the complete data set. The inferred temperature dependence of χ_i^{ANOM} is not inconsistent with that associated with either the ion mixing mode[69] or the trapped particle ubiquitous mode.[70] We note that the value of γ_0 reported above can also be applied to L-mode discharges on ASDEX.[71]

1.3.8 Electron Thermal Transport in Ohmic Experiments

The investigation of the electron thermal diffusion coefficient in ohmic toroidal experiments carried out in the past year has included the numerical simulation of the steady states of a number of ohmic toroidal experiments with circular cross section.[72] These included Alcators A and C, FT, ASDEX, TEXT, T-10, and TFTR. The ASDEX

---

66 R. Englade, submitted to *Nucl. Fusion* (1990).

67 R. Englade, *Nucl. Fusion* 29: 999 (1989).

68 R. Hawryluk, V. Arunasalam, M. Bell et al., in *Plasma Physics and Controlled Nuclear Fusion Research: Proceedings of the 11th International Conference,* Kyoto, 1986 (Vienna: IAEA, 1987), Vol. 1, p. 51; R. Goldston, V. Arunasalam, M. Bell et al., p. 75.

69 T. Antonsen, B. Coppi, and R. Englade, *Nucl. Fusion* 19: 641 (1979).

70 B. Coppi, MIT/RLE Report PTP-89/1 (Cambridge: MIT, 1989).

71 M. Keilhacker, G. Gierke, E. Müller et al, *Plasma Phys. Controlled Fusion* 28: 19 (1986).

72 L. Sugiyama, MIT/RLE Report PTP-89/3 (Cambridge: MIT, 1989).

cases included pellet-injected and improved ohmic confinement (IOC) phases as well as the corresponding "saturated" ohmic (SOC) phases. Similarly, Alcator C cases included pellet-injected and saturated ohmic phases, although here the pellet injected phase was not in steady state. The transport model assumed a Coppi-Mazzucato-Grüber electron thermal diffusion and neoclassical ion thermal diffusion. It correctly identified the cases where the ion thermal transport exceeded neoclassical (Alcator C and ASDEX saturated states).

In cases where the energy balance was dominated by the ohmic heating and the electron thermal diffusion, the CMG model gave a good fit to the experimental data. These included Alcator A at low q, FT, lower radiation TFTR cases, and one of the ASDEX pellet cases. The model predicted excess transport loss for cases where other losses were large — in particular, to some degree for all the ASDEX pellet and IOC cases, where radiation loss was large and centrally peaked (60 percent P_{OH}). Alcator A at high q, with higher radiation loss than the low q cases ($\sim$ 50 percent P_{OH}), was also poorly fit, although the experimental uncertainties in this case were relatively large. The single TEXT case could not be matched because a large particle inflow at the plasma edge and the corresponding density profile near the edge was difficult to fit with the simple model. The T-10 case behaved differently from the others and could not be fit; it has been suggested that charge exchange cause large thermal losses through the ions, consistent with the very low ion temperatures observed but not reproduced by the model.

In all cases except TFTR, only the purely ohmic form of the χ_e diffusion coefficient was used. Since it was derived by balancing the ohmic heating and the thermal diffusion, it is not surprising that it fits these cases best and that it overestimates the electron thermal transport when other losses, such as radiation, are important. One important result of the simulation is that the scaling adopted for the plasma voltage, V_ϕ is shown to fit a wide range of different experiments, particularly in the plasma dimensions, where the voltage ranges from less than unity to 2.6.

The results are consistent with the results from the analysis of the TFTR ohmic discharges, that the electron energy confinement time

$$\tau_{Ee} = W_e/P_{He} \equiv W_e/\ (P_{OH} - P_{RAD} - P_{ie})$$

does not have a good power law scaling with the plasma parameters except in the case when $P_{RAD} + P_{ie}$ is small, because the net heating P_{He} does not. In contrast, the total energy confinement $\tau_E = (W_e + W_i)/P_{OH}$ possesses a good power law scaling, for example, neo-Alcator $\bar{n}_e qR^2a$, although the exact powers cannot be determined too accurately. This state of affairs is consistent with the fundamental role of the loop voltage, and the existence of a good global scaling for it, in determining τ_E, but not τ_{Ee}. The loop voltage scaling, like the τ_E scaling, holds even for cases where radiation losses are large, but would be expected to break down when the ion thermal transport becomes large enough to affect the electron temperature and, therefore, the voltage. These conjectures, as well as an improved form for the CMG thermal diffusion, are being investigated. A test of the implications for the electron thermal transport of auxiliary heated discharges will also be made.

1.3.9 Combined Transport and Ray Tracing Studies of ECRF Heating in CIT

We have continued our fruitful collaboration with Dr. Miklos Porkolab, task leader for the assessment of electron cyclotron radio frequency (ECRF) heating prospects in the proposed Compact Ignition Tokamak (CIT). A 1 1/2 D equilibrium and transport code[73] in which thermal fluxes are expressed as the sum of an outward conduction term and an inward heat pinch and which models power deposition results obtained from a stand-alone ray tracing package has been used to

[73] M. Porkolab, P. Bonoli, R. Englade et al., 16th European Conference on Controlled Fusion and Plasma Physics, Venice, 1989.

study ECRF-assisted ignition scenarios for the most recent design parameters. These simulations take into account realistic start-up conditions in which current, magnetic field, and density are simultaneously ramped and the rays launched appropriately to maintain efficient plasma heating. Recently, we have made excellent progress in developing a large combined code in which the ECRF ray propagation and absorption, the MHD equilibrium calculation, and the plasma heat transport are treated self-consistently.[74] The ECRF package is a variation of the TORAY[75] toroidal ray tracing code, valid in both the Doppler and relativistic regimes. The values along a ray trajectory of the temperature, density, magnetic field components, and the derivatives of these quantities in a Cartesian coordinate system that are required inputs to TORAY have been obtained by a modification of the BALDUR 1 1/2 D equilibrium package utilized in[76] This modification makes extensive use of a procedure originally developed to track a chord through the nested flux surface geometry of a toroidal device.[77] Much work remains to be done on optimizing the combined code, reducing its use of computer resources, and installing necessary diagnostics. Based on the few trials performed so far, however, it is performing its basic functions as expected and has the potential to become a useful physics tool.

1.3.10 Studies of Advanced Fuel Fusion

Magnetic confinement geometries employing tight aspect ratios, high current densities, and high magnetic fields have long been proposed for the study of the ignition of deuterium-tritium plasmas and α-particle heating.[78] Recent work[79] on the Ignitor project in Europe has demonstrated in detail the feasibility of constructing such devices and suggested means of further increasing their operating pulse lengths and flexibility. Simultaneously, studies of the physics of the ignition process suggest that D-T ignition may be relatively easy to achieve.[80] These considerations have brought renewed interest (since 1980)[81] in the possibility of burning the so-called advanced fuels with significantly lower neutron yields than D-T, i.e., D – ^{3}He or D-D with an initial fueling of ^{3}HE, where 6–10 percent of the energy is produced in energetic neutrons for a 30 percent mixture of ^{3}He, compared to 80 percent for D-T.

We have developed[82] a 1D transport model that includes two ion species, the important D – ^{3}He and D-D cycle fusion reactions, and the synchrotron and bremsstrahlung radiation losses and applied it to the ignition problem. We have further investigated the character-

---

74 P. Bonoli, R. Englade, M. Porkolab et al., *Bull. Am. Phys. Soc.* 34:2133 (1989).

75 A. Kritz et al., *Proceedings of the Third International Symposium on Heating in Toroidal Plasmas,* Brussels, 1982, Vol. II, p. 707.

76 M. Porkolab, P. Bonoli, R. Englade et al., Sixteenth European Conference on Controlled Fusion and Plasma Physics, Venice (1989).

77 S. Attenburger, W. Houlberg, and S. Hirshman, *J. Comput. Phys.* 72:435 (1987).

78 B. Coppi, MIT/RLE Report PRR-75/18, MIT, 1975, and *Comm. Plasma Phys. Cont. Fusion* 3:2 (1977).

79 B. Coppi and L. Lanzavecchia, *Comm. Plasma Phys. Cont. Fusion* 11:47 (1987).

80 L. Sugiyama, MIT/RLE Report PTP-84/2 (Cambridge: MIT, 1984); R.C. Englade, *Nucl. Fusion* 29:999 (1989).

81 S. Atzeni and B. Coppi, *Comm. Plasma Phys. Cont. Fusion* 6:77 (1980); B. Coppi and G. Vlad, MIT/RLE Report PTP-82/16 (Cambridge: MIT, 1982); and G. Vlad, *Il Nuovo Cimento* 84B:141 (1984).

82 B. Coppi and L. Sugiyama, MIT/RLE Report PTP-88/6 (Cambridge: MIT, 1988), submitted to *Nucl. Fusion.*

istics of an experiment of the Candor[83] type and shown[84] that it may be possible to ignite in D-^{3}He, under "favorable" although still degraded conditions on the plasma thermal transport, with either an initial deuterium and tritium plasma and a moderate amount of auxiliary heating, or with no tritium and a much larger amount of auxiliary heating. Some of the major problems uncovered were the need to rapidly heat a fairly dense plasma from a few keV to some 70 keV and $\bar{n}_e \simeq 1.5 - 2 \times 10^{15}\ cm^{-3}$, and central control of the concentrations of the various nuclei, so that fuel nuclei can be added and the inert fusion products removed after they have slowed down in the plasma. The neutron production and the α-particle buildup may be significant if D-T burning is used to start the sequence, even with small amounts of initial tritium (10-15 percent). The plasma β may reach or exceed the first limit of stability to ideal MHD modes and means to control the transition to the second stability region may be necessary.

In the past year, work has focused on extending the analysis to include the effects of plasma geometry and finite beta,[85] by modifying a 1 1/2D transport simulation code, BALDUR, as developed by G. Bateman at PPPL. Concurrent work done on low beta DT ignition in a similar configuration suggests a number of areas to investigate, but we have not developed a consistent set of models valid for high beta yet. This work is continuing.

1.4 Investigation of Electron Cyclotron Resonance Plasma Production in the Versator II Tokamak

Sponsor

U.S. Department of Energy
Contract DE-AC02-ET-51013

Project Staff

Professor Miklos Porkolab, Dr. Kuo-In Chen, Dr. Stanley C. Luckhardt, Stefano Coda, Jeffrey A. Colborn, Edward W. Fitzgerald, Robert J. Kirkwood, Alberto Leon, Kurt A. Schroder, Jared P. Squire, Jesus N.S. Villasenor

During 1989, we investigated the characteristics of plasmas generated by RF and electron cyclotron resonance (ECR) in the Versator II device. These RF produced and sustained plasmas have important applications in the start-up phase of proposed large scale fusion power producing tokamaks such as ITER and CIT. These plasmas have potential use in applications as diverse as laboratory simulation of space and ionospheric plasmas, basic plasma turbulence studies, and plasma processing of materials. The principle distinction between RF sustained plasmas and standard tokamak plasmas is that the RF sustained plasmas have little or no net toroidal plasma current. The plasma confinement in the tokamak relies on a magnetic field configuration produced by a large current flowing in the plasma and a toroidal field supplied by external coils. In the case of the ECR sustained plasmas, little or no net plasma current flows, instead the plasma is confined by a combination of a toroidal field, a weak externally applied vertical field, and radial electric fields generated by plasma transport processes. Plasma theory suggests that these electric fields, in combination with the external magnetic fields, provide the surprisingly good plasma confinement observed in our experiments.

---

[83] Ibid.; B. Coppi, *Nucl. Instr. Methods Phys. Res.* A271:2 (1988).

[84] B. Coppi and L. Sugiyama, MIT/RLE Report PTP-88/6, MIT, 1988, submitted to *Nucl. Fusion.*

[85] L.E. Sugiyama, *Bull. Am. Phys. Soc.* 34:2171 (1989).

The aim of the present electron cyclotron heating experiments on Versator II is to (1) develop an understanding of the particle and energy transport, ionization processes, and single particle orbital confinement; (2) determine the characteristics of EC-ionized plasmas and their dependence on RF power levels and other parameters; (3) measure internal electric fields; and (4) investigate plasma currents that can be initiated by launching lower-hybrid waves into such plasmas.

Last year, we performed EC-ionization experiments on Versator-II using the NRL/MIT gyrotron, which produces 35.07 GHz microwaves in the circular TE_{10} mode. These microwaves are subsequently converted to the TE_{11} and then the HE_{11} mode.[86] In the present configuration, these linearly-polarized waves are launched perpendicularly to B_0 in the X-mode polarization from the high magnetic field side (inside) of the torus via a mirror. By rotating the mirror, we can vary the toroidal launch angle from − 60 degrees to + 60 degrees. The gyrotron is quite compact, requiring extensive modification of several of its components in a nearly-completed program to increase the pulse length and power level to 10−20 ms and 75−100 kW. For the data presented here, we achieved pulse lengths and power levels of 1−2 ms and 40−50 kW, and $B_0 = 1.25T$, placing the electron-cyclotron layer at the center of the vacuum chamber, which has $R_0 = 0.40m$ and a=0.13 m. In the experiments described below, a vertical field $B_v < 0.017T$ was applied, the vacuum chamber was prefilled with H_2 gas, and no gas was puffed in during the discharges. We measured density profiles along vertical chords using a radially-movable microwave interferometer, but measured the H_α light emission profiles vertically and horizontally by a movable detector that we placed on the bottom or side of the tokamak.

We found several phenomena in these initial experiments that were consistent with our theoretical interpretation. In the following, we summarize the results briefly. Figure 11 shows the time evolution of a typical EC-ionized discharge. The long decay-time of the electron density in these experiments, also shown in figure 11, in the absence of a measurable poloidal magnetic field is indicative of good plasma confinement. We believe this long delay time can be explained if there are internally generated radial electric fields in the plasma. We believe that a combination of the external magnetic field and internally generated electric fields and currents provides confinement of the plasma on a time scale much greater than the single particle drift time scale ~ 10 microseconds. As indicated by the H_α light emission (proportional to the hydrogen ionization rate), the ionization rate reaches a maximum about 0.5 ms into the EC pulse. Both of these features are roughly independent of applied B_v.

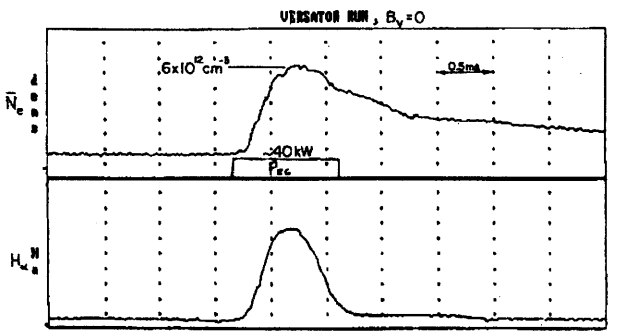

Figure 11. Time evolution of typical ECRH ionization plasma density and H_α light emission signals. The externally applied magnetic field is purely toroidal in this case.

The electron density as a function of time and radius (vertically chord-averaged) is shown in figure 12. The most notable feature is that, starting from very early in the discharge, the density peaks at a point between the cyclotron layer (at r=0) and the upper-hybrid layer. This is consistent with the

[86] S.C. Luckhardt et al., "Applications of Radio Frequency Power to Plasmas," in *Proceedings of the Seventh Topical Conference,* Kissimmee, Florida, 1987, p. 29.

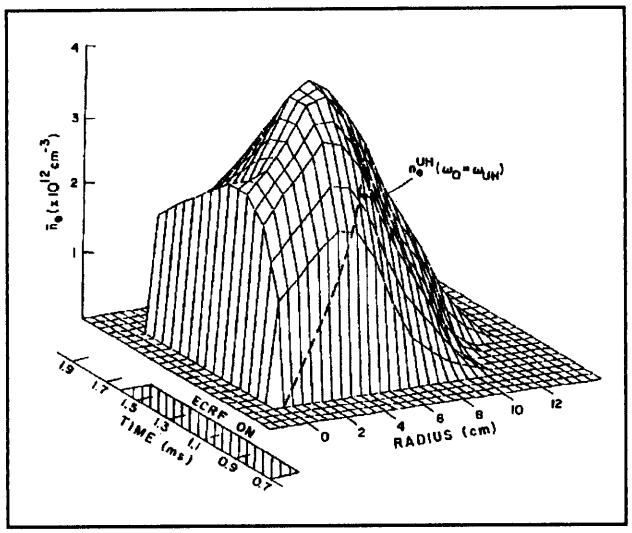

Figure 12. Time evolution of plasma density profiles during ECRH ionization.

findings of others.[87] Figure 13 shows the analogous plot for the H_α light emission. Note that the plot peaks sharply, shifting outward to a position near the upper-hybrid layer ($\omega = \omega_{UH}$) as the discharge progresses. These radial dependencies of the plasma density and H_α light emission are consistent with the currently accepted understanding of the plasma heating/ionization processes going on near the cyclotron resonance layer. That is, after a very low density plasma is formed at the cyclotron layer, the incident electromagnetic wave in the extraordinary mode is mode-converted at the upper-hybrid layer to electron Bernstein waves. These waves are locally damped and build up the plasma density and temperature near and on the inside of the upper-hybrid layer.[87]

The dependence of plasma density versus prefill Hydrogen pressure is shown in figure 14. The sharp absence of breakdown below fill pressures of $3-4 \times 10^5$ torr confirms the results of Anisimov et al., who worked on a very small device.[88] This feature can be explained by (1) equating the drift-confinement time of energetic electrons created by ECRH to the average time required for them to ionize neutrals, and (2) solving for the gas pressure below which the energetic electrons are lost before ionizing a significant number of neutrals. This minimum pressure is a function of ECRH power.

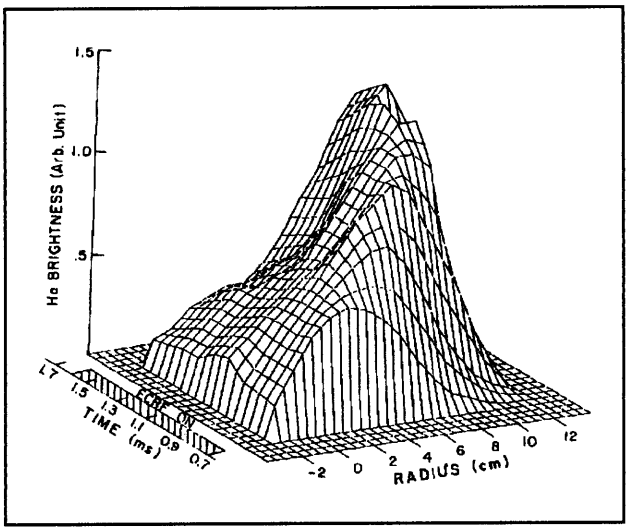

Figure 13. H_α light emission profiles during ECRH ionization.

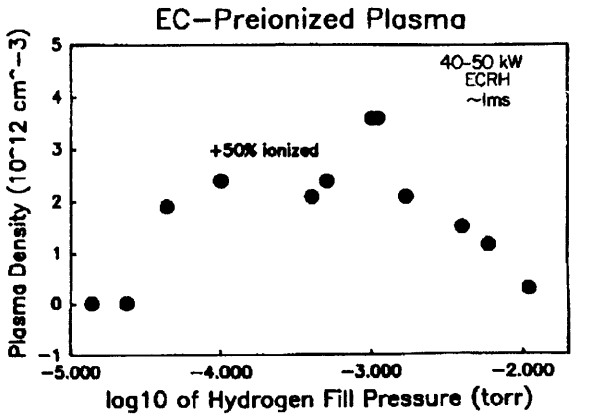

Figure 14. Dependence of peak plasma density on gas fill pressure, $P_{ECRH} = 50kW$.

[87] A.I. Anisimov et al., *Sov. Phys. Tech. Phys.* 16:546 (1971); R.M. Gilgenbach et al., *Nucl. Fus.* 12:319 (1981); T. Cho et al., *Nucl. Fus.* 26:349 (1986).

[88] A.I. Anisimov et al., *Sov. Phys. Tech. Phys.* 18:459 (1973).

Figure 15 shows the electron density during ECRH and 2 ms after ECRH turn-off as a function of applied vertical magnetic field. This data seems to indicate that confinement of the bulk plasma electrons is best when only a very small vertical field (<0.001 T) is present, and that the degradation in confinement that accompanies increased vertical field saturates near $B_v = 0.008T$.

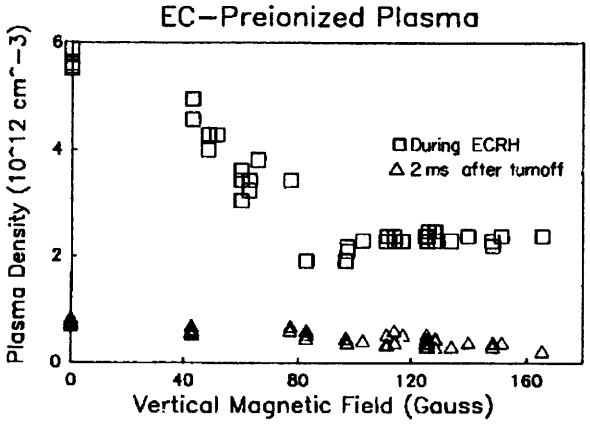

Figure 15. Dependence of plasma density on externally applied vertical magnetic field strength.